NASA TECHNICAL NOTE

NASA TN D-2210

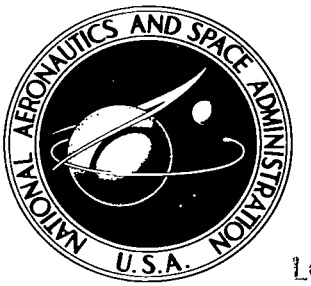

NASA TN D-2210

TWO-DIMENSIONAL FLUX AND CRITICALITY CALCULATIONS FOR THE PLUM BROOK REACTOR

by John H. Lynch

Lewis Research Center

Cleveland, Ohio

NATIONAL AERONAUTICS AND SPACE ADMINISTRATION • WASHINGTON, D. C. • OCTOBER 1964

TWO-DIMENSIONAL FLUX AND CRITICALITY CALCULATIONS FOR THE PLUM BROOK REACTOR

By John H. Lynch

Lewis Research Center
Cleveland, Ohio

NATIONAL AERONAUTICS AND SPACE ADMINISTRATION

For sale by the Office of Technical Services, Department of Commerce,
Washington, D.C. 20230 -- Price $1.25

TWO-DIMENSIONAL FLUX AND CRITICALITY CALCULATIONS FOR THE PLUM BROOK REACTOR

by John H. Lynch

Lewis Research Center

SUMMARY

A model has been developed to calculate reactor physics effects in the Plum Brook Reactor core, reflector, and test facilities. Results include calculated neutron fluxes in two dimensions and four energy groups and reactivity of the core with rods in, rods out, and at the cold clean measured critical height. The calculated power distributions agree with measured values; the calculated reactivities agree with measurements to within 2.0-percent reactivity ($\Delta K/K$) at all rod positions.

The prompt neutron lifetime and effective delayed neutron fraction were calculated, using the two-dimensional model, to be 57 microseconds and 0.00766, respectively.

Spatial flux distributions in four energy groups are presented in the form of two-dimensional isoflux maps in order to provide the maximum amount of information using a minimum of space. The results reported here correspond to a core loading consisting of 22 fixed elements, each having 168 grams of U-235, and five control rod follower elements, each having 131 grams of U-235. Current operating practice dictates the use of a mixture of new and partially depleted 200-gram (fixed) and 155-gram (follower) elements, which will yield a charge life of approximately 420 megawatt-days. Comparison calculations of mixed loadings have shown, however, that the unperturbed fluxes in the test holes and reflectors differ by less than 30 percent from the values presented in this report.

INTRODUCTION

During the initial design phase of the Plum Brook Reactor (PBR) there were no digital computer codes of the kind now widely available for reactor calculations. An analog simulator was used to perform calculations necessary for the hazards analysis of the reactor. These calculations were adequate for the reactor design, but the limited capabilities of the simulator precluded obtaining information on the effects of control rod positioning and limited the number of neutron energy groups to two: thermal and total epithermal.

The purpose of the work described in this report was to analyze the PBR using an improved calculational model. This model describes control rod effects on neutron fluxes and physics parameters and gives neutron fluxes in several energy groups, including one group above 0.821 Mev (since this energy range is of special interest with respect to radiation damage). It also allows rapid calculation of flux and reactivity effects of experiments to be inserted into the test facilities.

This report first describes the essential features of the model and the supplementary calculations done to establish its adequacy. This is followed by comparisons of flux and reactivity calculations with available experimental data and by a brief discussion of the accuracy of the model in calculating reactivity effects. Finally, kinetics parameters obtained from these calculations are given, and a brief derivation of the equations used to generate these parameters is shown in appendix B. The results of spatial flux calculations are presented as isoflux maps in order to provide the maximum amount of information to personnel associated with the reactor and the experiments for the reactor.

THE MODEL

The TWENTY GRAND (ref. 1) program developed at Oak Ridge was used for these calculations. This method of solution is an extension of the EQUIPOISE (ref. 2) method and solves the finite difference analogs of the neutron diffusion equations for several geometries and few-group energy descriptions over a two-dimensional array of mesh points.

Detailed drawings of the core are given in figures 1 and 2. The calculational representation of the core shown in figure 3 was adopted for the vertical calculations to be discussed in this section. This geometry was chosen because the reflectors and through holes (represented as squares to conserve mesh points) and the spatial dependence of the flux on shim rod positioning are treated explicitly. Atom densities, homogenized over the fueled core dimension in the east-west direction for this geometry, are shown in table I.

A four-group energy treatment was selected for these calculations so that the thermal and resonance regions and the flux above 1 Mev could be well defined. Although no important large resonances are present in the PBR materials, this flexibility was felt necessary in anticipation of experimental materials having such resonances. The lower limit for the highest energy group was chosen as 0.821 Mev, since this was the nearest energy breakpoint below 1 Mev of those available in the slowing-down code used to generate fast cross sections (ref. 3). An upper limit for the resonance region of 5.55 Kev was felt to include significant resonances in most materials. Since the core contains only about 4.4 kilograms of U-235, a Maxwellian thermal treatment was adopted. The thermal cutoff used was 5Kt (0.125 ev). This selection has been shown to give good experimental results for solution reactors having roughly the same U-235 to moderator atom ratios as the PBR (ref. 3).

Cross sections used in the neutron diffusion model were obtained from a

space-independent 450-lethargy-group, consistent-P_1, slowing-down analysis programmed for the IBM-7090 (ref. 3). A comparison calculation was also performed using the 54-group MUFT IV code (ref. 4). Disagreements were resolved to differences in measured cross-section data, which were corrected in favor of the MUFT data since MUFT is generally available and as such can be used to extend these calculations consistently. A one-dimensional P_5 calculation was used to obtain fuel-plate disadvantage factors. The cross sections so obtained are tabulated in table II.

The core geometry precluded any explicit control rod representation, since the control elements alternate with fixed fuel elements, and when viewed from the core end, as in figure 3, the effect of the rods on the flux profile was not immediately apparent. It was assumed that the effect of the control rods is predominantly absorptive, rather than to induce leakage at remote boundaries due to a spatial flux rearrangement. Under this assumption, and since the configuration does not lend itself to any realistic geometrical interpretation, the presence of control rods was believed best represented by a thermal poison cross section $\Sigma_{p_{th}}$ distributed homogeneously over the LC row above the rod height interface. This poison cross section was calculated in the following manner.

A two-dimensional four-group diffusion theory cell calculation was performed having the geometry shown in figure 4. This calculation simulated a horizontal slice of the core above the control rod interface. The cross sections used in this calculation were the same as those previously discussed. The fast absorption in cadmium was set to zero; the thermal absorption in cadmium was treated with blackness theory, by making use of the log-derivative boundary condition. A zero value of the vertical buckling was employed in all regions. If it is assumed that

$$\underset{\text{(with explicit rod)}}{\int_R \varphi_{th}\, dV} \equiv \underset{\text{(with } \Sigma_{p_{th}})}{\int_R \varphi_{th}\, dV} \tag{1}$$

where R denotes the region representing the fueled LC row in the cell geometry, the induced leakage effects are ignored, and the total captures in a control rod are conserved and distributed over R by defining the poison cross section as

$$\Sigma_{p_{th}} \equiv \frac{\int_{\text{rod volume}} \Sigma_{a_{th}} \varphi_{th}\, dV}{\int_R \varphi_{th}\, dV}. \tag{2}$$

The numerator of this expression is equal to the capture rate in the rod. By assuming negligible slowing down in the cadmium, the neutron balance for the control rod becomes

$$-\int \nabla \cdot D_{th} \nabla \varphi_{th} \, dV + \Sigma_{a_{th}}^{rod} \int \varphi_{th} \, dV = 0 \tag{3}$$

This may be transformed to

$$\Sigma_{a_{th}}^{rod} \int \varphi_{th} \, dV = \int D_{th} \nabla \varphi_{th} \, dS \tag{4}$$

(rod volume) (rod surface)

Cadmium was assumed to be black in this calculation; hence,

$$D_{th} = \frac{0.4695 \, \varphi_{th}}{\nabla \varphi_{th}} \tag{5}$$

at the rod surface. Substituting this into equation (4) yields the following expression for $\Sigma_{p_{th}}$:

$$\Sigma_{p_{th}} = \frac{0.4695 \int_{\text{rod surface}} \varphi_{th} \, dS}{\int_{R} \varphi_{th} \, dV} \tag{6}$$

which is easily obtained from the two-dimensional cell-flux solution.

Because of the selection of a thermal upper limit that is below the cadmium cutoff (0.4 ev), the epithermal rod absorption is significant. It was assumed that the thermal ratio of flux to current was also characteristic of the epithermal interval to cadmium cutoff ($16.5 \leq u \leq 18.2$). This allowed the epithermal rod absorptions to be treated as a correction to the thermal Σ_p. A correction factor, f, was defined as

$$f \equiv 1 + \frac{\int_{18.2}^{16.5} \varphi(u) \, du}{\int_{0}^{0.125} \varphi(E) \, dE} = 1.10 \tag{7}$$

which was evaluated using the fast flux spectrum of the adjacent fuel region from the slowing-down solution for this material. The $\Sigma_{p_{th}}$ generated in this manner was 0.09717 centimeter^{-1}.

A one-dimensional study was made of the east-west leakage properties of the core and reflectors in order to obtain a transverse buckling description

for the vertical two-dimensional calculations. The results of this study indicated that a geometric buckling of 0.9954×10^{-3} (based on the active core length plus a total reflector savings of 24.44 cm resulting from 3 in. of beryllium and an infinite water reflector) used in the fueled core regions, with zero buckling in nonfuel regions, satisfactorily described the east-west dimension.

CONFIRMATION OF THE MODEL

There was some doubt at first as to the feasibility of using a conventional few-group diffusion model for these calculations since the regions of main interest (experimental facilities) are external to the core (figs. 1 and 2). Also, since the fueled core is only about 9 inches thick in the north-south dimension, it was not clear that an asymptotic space-independent slowing-down model could be used to determine the required few-group cross sections. This was studied by comparing fluxes from a few-group one-dimensional (north-south) calculation with those from a multigroup calculation having the same geometry.

The one-dimensional IBM 7090 program employed solves the consistent P_1 approximation to the Boltzmann transport equation in 70 lethargy groups above thermal, with one additional group representing the thermal range. The group structure for this calculation is shown in table III. Atom densities were homogenized over each east-west row of elements in both the core and reflectors, and the traverse was taken in the north-south direction with rods withdrawn.

A comparison was made between the fueled core spectrum given by this 71-group space-dependent calculation and the spectrum given by a 450-group space-independent P_1 solution such as would be used to obtain few-group cross sections. Good agreement was observed to exist (fig. 5). To determine whether a few-group approach would correctly represent the spectra and the group flux distributions in the reflectors, a one-dimensional four-group calculation using space-independent cross-sections was performed having the same characteristics (geometry, mesh, boundary conditions, etc.) as the detailed 71-group calculation. No significant difference could be detected, over all core and reflector regions, between the fluxes from the four-group calculation and the equivalent integrals from the 71-group solution.

In figure 5 it can be seen that the two salient features of the fueled-core slowing-down fluxes (shape and integral) are in agreement. From this it was concluded that the space-independent cross sections obtained from the slowing-down model would represent the core accurately. The agreement between the 71-group and the equivalent four-group calculations in both core and reflectors demonstrated the spectral accuracy of the four-group approach and justified adopting this model for use in the subsequent analysis.

A vertical two-dimensional calculation was performed that described the clean critical configuration with shim rods numbers 1 through 5 at 15.3 inches, which is the normal configuration for reactor startup when the core loading is approximately 4.4 kilograms of U-235 (ref. 1). As additional confirmation of

the model, a plot of the thermal flux obtained from this calculation has been constructed (fig. 6). Values obtained from measurements (ref. 5) are shown for comparison. Figure 7 shows the calculated flux above 0.821 Mev compared to a measured traverse of nickel foil activations interpreted as above 1 Mev flux. The curves shown agree in the core and in the first two reflector rows outside the core. The deviation of the measured fast values from an exponential attenuation after the first two rows is attributed to the hardening in the fast neutron spectrum above 1 Mev, which was not accounted for in the measurements. It is expected that correction of the measurements for spectral effects would tend to make the attenuation nearly exponential, as in the calculated traverse.

An additional vertical calculation was performed that featured fully withdrawn control rods with natural boron in the fueled-core regions. The quantity (31.504 g) and distribution of boron was determined from a critical experiment performed for the purpose of calibrating control rods (ref. 5). The boron was represented in the calculation as a thermal absorber only, with calculated self-shielding corrections. An eigenvalue correction for the above thermal boron capture was derived with a change assumed only in the probability of fast capture escape (four-factor theory with constant leakage) and was evaluated with a $1/E$ dependence of the flux above thermal.

In addition to the two calculations just mentioned, a vertical calculation with all rods out was performed for the purpose of determining the core excess reactivity. A summary of eigenvalues for these vertical two-dimensional calculations is presented in the following table:

Description of calculation	Eigenvalue	Measured K_{eff}
(1) Clean critical; shim rod numbers 1 through 5 bank at 15.3 in.	1.0003	1.0000
(2a) Rods out critical; with boron	1.0258	1.0000
(2b) Same as (2a) but corrected for fast captures in boron	1.0164	1.0000
(3) Rods out; no boron	1.1605	------

The reactivity worth of the boron, obtained from calculations (2b) and (3), was 12.2-percent $\Delta K/K$ as compared to a value of 12.0-percent $\Delta K/K$ inferred from critical shim bank height measurements for several different boron loadings (ref. 5). Since the boron worth appears correct, the model without control rods is presumed to be positively biased by about $1\frac{1}{2}$ percent in the eigenvalues. This may be due to the use of zero transverse leakage in the reflector regions. In the clean critical calculation this effect may have been counteracted by a slight overestimate of the control rod Σ_p value. The adequacy of the control rod representation, however, and the utility of the model

with respect to heat-transfer analysis is demonstrated by the comparison of calculated and measured vertical power distributions in the LD row (fig. 8).

Calculation (1) was rerun with HT-1 represented as a void using Wachspress's method (ref. 6). This technique represents voided tubes by a diffusion coefficient in all groups defined by

$$D_{void} = \frac{\text{radius of tube}}{2}\left[\ln\left(\frac{\text{length of tube}}{\text{radius of tube}}\right) - 0.705\right]$$

with Σ^A, Σ^R, and $\nu\Sigma^F$ in all groups set to zero. This description, when used with the core B_z^2, correctly represents the end leakage from the voided tube, which would be grossly overestimated if an arbitrarily large value of D were to be used as would seem intuitively correct. The calculated reactivity effect was 0.53-percent $\Delta K/K$ as compared to 0.46 percent $\Delta K/K$ measured.

A horizontal core calculation (geometry shown in fig. 21) was performed that described experiment capsules inserted in the LA-5 and LA-7 positions. A cell problem was used to obtain effective homogenized constants for the core problem. The reactivity effect was calculated to be -1.26-percent $\Delta K/K$ as compared to a measured value of -1.64-percent $\Delta K/K$.

The flux comparisons together with the reactivity effects and spectrum properties just discussed tend to confirm the model and to substantiate the results.

RESULTS

A vertical calculation was performed with fuel shim rods 1 through 5 fully inserted, which gave an eigenvalue of 0.8402. The shutdown reactivity of shim rods 1 through 5 obtained from this calculation and the clean critical calculation was 19.0-percent $\Delta K/K$. The excess reactivity was taken to be the reactivity worth of the boron or 12.2-percent $\Delta K/K$.

Figures 9 through 12 show the spectrum from the 71-group one-dimensional calculation at various locations outside the fueled core. The calculated spectrum in the LC row, characteristic of the core spectrum, is also shown on each plot so that departures from this may be readily assessed. The fast spectral hardening in the reflector, mentioned previously, is apparent from these comparisons.

Table IV summarizes the calculated fluxes in the test holes and at other points of interest in the reflector. The effect of control rods on flux distribution is evident. This table may be interpreted as showing the limits of flux variations over one fuel charge life with a continuous, monotonic, time-dependent variation of the point-wise flux assumed in each group. It is possible to infer from this table the relative merit of several facilities, depending on experimental flux level and flux variation tolerances. For example, HT-1 appears to be the prime facility for larger experiments since the fluxes are high and the flux variation over core lifetime is small. For small experiments, however, it can be seen that the LA row at the core midplane is prefer-

able since the fluxes are higher and the variation is only a few percent. The RA positions appear to be preferable to the RB positions for the same reasons. Similarly, at the south face of the core, HB-4 and HB-5 tend to be preferable to HB-6 if the previous criteria alone are considered.

Flux distributions by energy group for the critical (rods at 15.3 in.) case and for the "rods out with boron" case are displayed in figures 13 to 20. These isoflux maps were constructed to provide a readable and complete presentation of the output of the computer calculations. The maps were made by plotting one-dimensional distributions from the output. Points of equal flux were then transcribed from these one-dimensional distributions to the two-dimensional isoflux maps. This eliminated the need for any interpolation of flux values and enabled the calculated results to be presented correctly. It should be noted here that these maps are for beryllium shim rods and regulating rods fully withdrawn to 30.9 inches, while operating procedure calls for one regulating rod at 50-percent insertion with beryllium shim rods at 28.0 inches.

In order to provide a more complete description of the flux distributions, one horizontal plane calculation, poisoned as in vertical calculation (2a) but having the geometrical layout shown in figure 21, was performed which is descriptive of a vertical average of the core materials. Four group fluxes from this calculation appear in figures 22 to 25. Quarter core symmetry was assumed for this calculation since the inability to represent the through hole (HT-1) explicitly tends to underestimate the flux gradients in the R lattice. Measurements have shown that the fueled core fluxes are essentially symmetric in both east-west and north-south directions (ref. 5).

To provide a more complete description of the nuclear characteristics of the PBR, some mention must be made of the kinetic parameters of the reactor. By using the perturbation theory approach derived in appendix B, values for Λ, the prompt neutron lifetime, and $\bar{\beta}$, the effective delayed neutron fraction, were calculated to be 5.7×10^{-5} second and 0.00766, respectively, (where β absolute is 0.0064).

Detailed measurements of $\bar{\beta}$ for the BSR-I (ref. 7) have given a value of 0.00800 for 140-gram fuel elements similar to those used in the PBR (which has 168-gram elements) but arranged in a five-by-five lattice. It is encouraging to see that this value is in fairly good agreement with that calculated for the PBR. The difference may be due to geometry; more neutrons producing fission experience their moderation in the reflectors in the PBR. The calculated value for the PBR was further substantiated using an elementary four-factor model having that gross buckling associated with the 15.3-inch critical rod bank height. This model gave a value of 0.00768, which, although possibly fortuitous, tends to substantiate the more elaborately obtained results.

A lack of experimental data precludes confirmation of the calculated prompt neutron lifetime; however, the model used is consistent with that used in determining $\bar{\beta}$, so that it is reasonable to expect similar accuracy here.

CONCLUDING REMARKS

A reliable model for calculating flux and reactivity effects in and around the PBR core has been developed, and results have been obtained that are of interest to both Plum Brook personnel and to sponsors of experiments for the Plum Brook Reactor (PBR). The information obtained agrees with results of the low-power tests described in reference 5. The calculational model will be a useful adjunct to the PBR experimental program and to the mockup reactor criticality measurements program.

Lewis Research Center
National Aeronautics and Space Administration
Cleveland, Ohio, June 29, 1964

APPENDIX A

SYMBOLS

A	four group diffusion matrix
A*	four group adjoint coefficient matrix
a	power normalization factor
B_z^2	geometric buckling transverse to dimensions solved
C_j	concentration of precursors from which j^{th} group of delayed neutrons arise
D	diffusion coefficient
E	energy
F	diffusion space flux vector
f	correction factor to account for fast cadmium absorption
I	nonfission matrix
I*	transposed nonfission matrix
J	fission matrix
J*	transposed fission matrix
K	multiplication constant
ΔK	change in multiplication constant
K_{ex}	excess multiplication, $K_{eff} - 1$
Kt	energy of 2200 m/s neutrons, 0.025 ev
P	asymptotic prompt period
P_1, P_5	spherical harmonics approximations to Boltzman transport equation
R	region representing fueled LC row in cell geometry
r	position vector denoting space dependence
dS	differential surface vector

$S_i(r,t), S_i(r)$	source of neutrons to i^{th} group
$\mathscr{V}$	volume of both reactor and reflectors
$T_i(t)$	time-dependent part of flux
t	time
u	lethargy
V	volume
$\overline{v}$	velocity of neutrons
β	measured delayed neutron fraction
$\overline{\beta}$	effective delayed neutron fraction
β_j	fraction of total number of fission neutrons that are delayed neutrons belonging to j^{th} group
δ	variation operator for constant time
$\eta(u)du$	number of neutrons having lethargy u in interval du about u
Λ	prompt neutron lifetime
λ	steady-state eigenvalue of unperturbed diffusion calculation
$\hat{\lambda}$	inverse of prompt period
λ_j	decay constant for j^{th} delayed neutron group
ν	average number of neutrons released per fission
$\nu\Sigma^F$	macroscopic fission cross section
ρ	reactivity
Σ^A	macroscopic absorption cross section
Σ^R	macroscopic removal (by scattering) cross section
$\Sigma_{a_{th}}^{rod}$	macroscopic thermal absorption cross section of control rod
$\Sigma_{p_{th}}$	homogeneous macroscopic thermal poison cross section used to represent control rods
Φ	four group flux vector
φ	neutron flux

$\varphi(E)$ neutron flux as function of energy

$\varphi(u)$ neutron flux as function of lethargy

φ_{th} Maxwellian thermal flux

χ_i fraction of fission neutrons born into ith energy group

$\underline{\Psi}^*$ four group adjoint flux vector

Subscripts:

eff effective

i index denoting energy flux group 1, 2, 3, or 4

j index denoting delayed neutron group 1, 2, 3, 4, 5, or 6

M Maxwellian

th thermal

0 denotes steady state

APPENDIX B

DERIVATION OF THE KINETICS PARAMETERS

To generate the prompt neutron lifetime Λ and the effective delayed neutron fraction $\bar{\beta}$, a perturbation theory analysis was used that employs fluxes and adjoint fluxes from the two-dimensional criticality calculation having rods at 15.3 inches.

The prompt neutron lifetime is derived in the following manner. The space- and time-dependent diffusion equations for any energy group i are written

$$\nabla \cdot D_i \nabla \varphi_i(r,t) - \left(\Sigma_i^A + D_i B_z^2 + \Sigma_i^R\right)\varphi_i(r,t) + S_i(r,t) = \frac{1}{\bar{\bar{v}}_i} \frac{\partial \varphi_i(r,t)}{\partial t} \tag{B1}$$

It can be shown (ref. 8) that

$$\varphi_i(r,t) = a\varphi_i(r)e^{K_{ex}t/\Lambda} \tag{B2}$$

Inherent in this expression are the assumptions of a unique eigenfunction solution and space-time separability of the flux, stated mathematically as

$$\varphi_l(r,t) = \varphi_l(r)T_i(t) \tag{B3}$$

Substituting this flux form into the diffusion equations just given and observing that

$$\frac{1}{\bar{\bar{v}}_i} \frac{\partial \varphi_i(r,t)}{\partial t} = \frac{\varphi_i(r)}{\bar{v}_i} \frac{\partial T_i(t)}{\partial t} = \frac{\varphi_i(r)T_i(t)}{\bar{v}_i} \frac{K_{ex}}{\Lambda} \tag{B4}$$

yields

$$\nabla \cdot D_i \nabla \varphi_i(r) - \left(\Sigma_i^A + D_i B_z^2 + \Sigma_i^R\right)\varphi_i(r) + S_i(r) = \frac{1}{\bar{v}_i} \frac{K_{ex}}{\Lambda} \varphi_i(r) \tag{B5}$$

If the reactor is on an asymptotic prompt period P the inverse of this period is a constant, which will be defined herein as

$$\hat{\lambda} \equiv \frac{1}{P} = \frac{K_{ex}}{\Lambda} \tag{B6}$$

This term can be transposed to the left side of the revised diffusion equation (B5) so that it appears as an additional absorption. Then

$$\nabla \cdot D_i \nabla \varphi_i(r) - \left(\Sigma_i^A + D_i B_z^2 + \Sigma_i^R + \frac{\hat{\lambda}}{\bar{v}_i}\right)\varphi_i(r) + S_i(r) = 0 \qquad \text{(B7)}$$

the solution of which may be obtained by a steady-state analysis. The eigenvalue corresponding to this solution will be the multiplication after some arbitrary absorber equal to $\hat{\lambda}/\bar{v}_i$ is inserted.

This perturbation was made over the core and all reflectors, since neutrons in the reflectors have a finite probability of returning to the core and thus affect the averaging of the prompt neutron lifetime. The lifetime is related to the perturbed and unperturbed calculations by

$$\Lambda = \frac{\Delta K/K}{\hat{\lambda}} \qquad \text{(B8)}$$

The prompt neutron lifetime is obtained by calculating $\Delta K/K$ from criticality for a given $\hat{\lambda}/\bar{v}_i$ in each group. This was handled using perturbation theory, where the reactivity change is given by

$$\frac{\delta K}{K} = \frac{\int_{\mathcal{S}} \underline{\bar{\psi}}_0^* \delta I \Phi_0 - \nu \int_{\mathcal{S}} \underline{\bar{\psi}}_0^* \delta J \Phi}{\nu \int_{\mathcal{S}} \underline{\bar{\psi}}_0^* J \Phi_0} \qquad \text{(B9)}$$

where $\mathcal{S}$ denotes the volume of both reactor and reflectors. This form arises from an arrangement of the group diffusion equations with all nonfission terms written on the left and all the fission source terms (groups 1 and 2 only) written on the right. Their matrix form is then

$$I\Phi_0 = \nu J \Phi_0 \qquad \text{(B10)}$$

where J and I are the fission and nonfission matrices. The terms Φ_0 and $\underline{\bar{\psi}}_0^*$ are those flux and adjoint flux vectors that are obtained from the unperturbed steady-state flux and adjoint flux solutions, the adjoints being the flux solutions in the same geometry but defined by

$$I^* \underline{\bar{\psi}}_0^* = \nu J^* \underline{\bar{\psi}}_0^* \qquad \text{(B11)}$$

where I^* and J^* are the transposed matrices of I and J. In this case δJ is a null matrix since no perturbation was made to the fission source, while δI is a diagonal perturbation matrix, having as elements the $\hat{\lambda}/\bar{v}_i$ in each group. As can be seen from equations (B8) and (B9), the calculation is independent of $\hat{\lambda}$, which in this case was conveniently chosen as 1.0, so that $\Lambda = \Delta K/K$. The $\bar{v}_i$ (average velocity of the neutrons in the i^{th} group) were calculated from the slowing down solution for the core materials using

$$\bar{v}_i = \frac{\int_i \varphi(u)\,du}{\int_i \eta(u)\,du} \tag{B12}$$

for the fast groups and $\bar{v}_M$ for the thermal group. Assuming the same group average velocities to prevail outside the core tends to be conservative because it decreases the calculated prompt neutron lifetime slightly. The magnitude of the flux-adjoint product integrals in the reflector indicated, however, that exploration of the uncertainty so introduced was unnecessary.

The ratio of the effective delayed neutron fraction $\bar{\beta}$ to the total measured delayed neutron fraction, commonly referred to as β, was obtained using a similar technique. The functional form of $\bar{\beta}$ was obtained from the first kinetics equation (B21) as derived from perturbation considerations. A brief outline of this procedure, intended only to provide continuity of argument, is given here. For a more expansive discussion of the manipulations outlined, reference 9 is one of the more authoritative treatises in this area.

The four-group diffusion equations for steady-state criticality are written

$$A_0\Phi_0 = 0 \tag{B13}$$

where $A_0 = I_0 - \nu J_0$. In order to account for delayed neutrons (all born into the second group), the second-group equation is written, neglecting flux arguments, as

$$\nabla \cdot D_2\nabla\varphi_2 - \Sigma_2^A\varphi_2 + \sum_j C_j\lambda_j - \Sigma_2^R\varphi_2 + \Sigma_1^R\varphi_1 + \chi_2 \sum_{i=1}^{4} \nu\Sigma_i^F\varphi_i\left(\frac{\chi_2 - \beta}{\chi_2}\right) = 0 \tag{B14}$$

where χ_2 is the second-group fission integral. The adjoint equations, obtained by taking the transpose of A_0, are described by

$$A_0^*\bar{\Psi}_0^* = 0 \tag{B15}$$

If the reactor experiences a change in composition such that one or more of the elements of A_0 is changed, the defining equation is

$$A\Phi = \frac{\partial}{\partial t}\begin{pmatrix} \varphi_1/\bar{v}_1 \\ \varphi_2/\bar{v}_2 \\ \varphi_3/\bar{v}_3 \\ \varphi_4/\bar{v}_4 \end{pmatrix} \tag{B16}$$

where the zero subscript has been dropped to denote departure from steady state. Now the perturbed equations are multiplied by the steady-state adjoint fluxes and the steady-state adjoint equations by the perturbed fluxes and then the latter are subtracted from the former and the result is integrated over the reactor volume. Symbolically this is written

$$\int_R (\underline{\bar{\psi}}_0^* A\Phi - \Phi A_0^* \underline{\bar{\psi}}_0^*) = \int_R \underline{\bar{\psi}}_0^* \left[\frac{\partial}{\partial t} \begin{pmatrix} \varphi_1/\bar{v}_1 \\ \varphi_2/\bar{v}_2 \\ \varphi_3/\bar{v}_3 \\ \varphi_4/\bar{v}_4 \end{pmatrix} \right] \tag{B17}$$

Assuming time-space separability of the flux results in

$$\varphi_i(r,t) = \varphi_i(r) T_i(t) \tag{B18}$$

The time-dependent part of the flux $T_i(t)$ is chosen the same for all groups and will be described here using conventional notation as $T_i(t) = T$. Denoting the diffusion space flux vector by

$$F = \begin{bmatrix} \varphi_1(r) \\ \varphi_2(r) \\ \varphi_3(r) \\ \varphi_4(r) \end{bmatrix} \tag{B19}$$

allows equation (B17) to be written as

$$\int_R (\underline{\bar{\psi}}_0^* AF - FA_0^* \underline{\bar{\psi}}_0^*) = \int_R \underline{\bar{\psi}}_0^* \left\{ \begin{bmatrix} \varphi_1(r)/\bar{v}_1 \\ \varphi_2(r)/\bar{v}_2 \\ \varphi_3(r)/\bar{v}_3 \\ \varphi_4(r)/\bar{v}_4 \end{bmatrix} \frac{1}{T} \frac{\partial T}{\partial t} \right\} \tag{B20}$$

the second term on the left being zero by equation (B15). Carrying out the indicated operations yields a complicated expression that can be interpreted as the first kinetics equation

$$\frac{dT}{dt} = \frac{\rho - \bar{\beta}}{\Lambda} T - \sum_j \lambda_j C_j = 0 \tag{B21}$$

where the term recognized as $\bar{\beta}$ is

$$\bar{\beta} = \frac{\left(\sum_j\right) \beta_j \int_R \psi^*_{2,0} \sum_{i=1}^{4} \frac{\nu}{\lambda} \Sigma^F_i \varphi_{i,0} \, dv}{\int_R (\psi^*_{1,0} \chi_1 + \psi^*_{2,0} \chi_2) \sum_{i=1}^{4} (\nu \Sigma^F_i \varphi_{i,0}) dv} \tag{B22}$$

The prompt neutron lifetime Λ obtained as indicated is identical in form to the expression derived by the direct $1/\bar{v}_i$ perturbation method and, hence, can be considered consistent in derivation with $\bar{\beta}$. The form of the other terms in equation (B21) are of no immediate interest.

REFERENCES

1. Tobias, M. L., and Fowler, T. B.: The TWENTY GRAND Program for the Numerical Solution of the Few-Group Neutron Diffusion Equations in Two Dimensions. ORNL-3200, AEC, Feb. 21, 1962.

2. Tobias, M. L., and Fowler, T. B.: EQUIPOISE - An IBM-704 Code for the Solution of Two Group, Two Dimensional Neutron Diffusion Equations in Cylindrical Geometry. ORNL-2967, AEC, Oct. 17, 1960.

3. Fieno, Daniel: Consistent P1 Analysis of Aqueous Uranium-235 Critical Assemblies. NASA TN D-1102, 1961.

4. Bohl, Henry, Gelbard, Ely M., and Ryan, Georgia H.: MUFT-4 - A Fast Neutron Spectrum Code for the IBM-704. WAPD-TM-72, AEC, July 1957.

5. Giesler, Harold W., Reilly, Harry J., and Poley, William A.: Low-Power Tests of the Plum Brook Reactor. NASA TN D-1560, 1963.

6. Wachspress, E. L.: Two Dimensional r-θ Multigroup. KAPL-1172, AEC, Aug. 16, 1954.

7. Perez-Belles, R., Kington, J. D., and deSaussure, G.: A Measurement of the Effective Delayed Neutron Fraction for the Bulk Shielding Reactor-I. Nuclear Sci. and Eng., vol. 12, no. 4, Apr. 1962, pp. 505-512.

8. Glasstone, Samuel, and Edlund, Milton C.: The Elements of Nuclear Reactor Theory. D. Van Nostrand Co., Inc., 1956.

9. Henry, A. F.: Computations of Parameters Appearing in the Reactor Kinetics Equations. WAPD-TM-142, AEC, Dec. 1955.

TABLE I. - HOMOGENIZED ATOM DENSITIES FOR GEOMETRIES SHOWN IN FIGURES 3 AND 21

Composition	Element									
	Hydrogen	Oxygen	Aluminum	Beryllium	Uranium		Iron	Chromium	Nickel	Carbon
					235	238				
	Atom density, atoms/cm^3									
1	0.0390×10^{24}	0.0195×10^{24}	0.025×10^{24}	----------	0.0001055×10^{24}	0.0000076×10^{24}	----------	----------	----------	----------
2	.0368	.0184	.0271	----------	.00009248	.0000067	----------	----------	----------	----------
3	.00634	.00317	----------	0.1117×10^{24}	----------	----------	----------	----------	----------	----------
4	.0529	.0265	.0127	----------	----------	----------	----------	----------	----------	----------
5	.0482	.0241	.0054	----------	----------	----------	0.0092×10^{24}	0.0026×10^{24}	0.0012×10^{24}	----------
6	.0313	.0156	----------	.0170	----------	----------	.0219	.0062	.0027	0.0001×10^{24}
7	.0468	.0234	.0175	----------	----------	----------	.0006	.0002	.0001	----------
8	.0230	.0115	.0230	.0501	----------	----------	.0030	.0009	.0004	----------
9	.0421	.0211	.0223	----------	----------	----------	----------	----------	----------	----------
10	.0074	.0037	----------	.1099	----------	----------	----------	----------	----------	----------
11	.0194	.0097	----------	----------	----------	----------	.0434	.0124	.0055	.0002
12	.0161	.0080	.0458	----------	----------	----------	----------	----------	----------	----------
13	.0669	.0334	----------	----------	----------	----------	----------	----------	----------	----------
14	.0067	.0033	----------	.1113	----------	----------	----------	----------	----------	----------
15	.0057	.0028	----------	.1131	----------	----------	----------	----------	----------	----------
16	.0294	.0147	.0133	.0242	----------	----------	.0089	.0026	.0011	----------
17	.0442	.0221	.0127	----------	----------	----------	.0080	.0023	.0010	----------
18	.0406	.0203	.0232	----------	.00004689	.000003377	.00048	.00016	.00007	----------
19	.0420	.0210	.0113	----------	.00004689	.000003377	.00906	.00255	.0113	----------
20	.0391	.0196	.0257	----------	.00004559	.000003283	----------	----------	----------	----------
21	.0351	.0176	.0287	----------	.00008206	.00000591	----------	----------	----------	----------

TABLE II. - SUMMARY OF CONSTANTS AVERAGED OVER COMPOSITIONS SHOWN IN FIGURES 3 AND 21

Composition	Group	Diffusion coefficient, D	Macroscopic absorption cross section, Σ^A	Macroscopic removal cross section, Σ^R	Macroscopic fission cross section, $\nu\Sigma^F$	Composition	Group	Diffusion coefficient, D	Macroscopic absorption cross section, Σ^A	Macroscopic removal cross section, Σ^R	Macroscopic fission cross section, $\nu\Sigma^F$
1	1	2.342974	0.000513	0.070869	0.000389	12	1	2.637846	0.000240	0.039104	--------
	2	1.258146	.000312	.087404	.000508		2	1.582554	.000108	.037259	--------
	3	.890750	.007795	.072449	.011452		3	1.642761	.001174	.031162	--------
	4	.236936	.080505	--------	.131939		4	.545151	.014072	--------	--------
2	1	2.365684	0.000484	0.067934	0.000341	13	1	2.133330	0.000509	0.106381	--------
	2	1.276812	.000286	.082587	.000446		2	1.105613	.000005	.148303	--------
	3	.931102	.006995	.068585	.010061		3	.591455	.001662	.130807	--------
	4	.250867	.072437	--------	.115779		4	.149612	.019624	--------	--------
3	1	1.993934	0.004391	0.050958	--------	14	1	1.991029	0.004382	0.051281	--------
	2	.618326	.000001	.038289	--------		2	.619149	.000001	.038787	--------
	3	.493531	.000258	.025159	--------		3	.493390	.000265	.025641	--------
	4	.357731	.002882	--------	--------		4	.355280	.002958	--------	--------
4	1	2.229918	0.000441	0.088916	--------	15	1	1.997218	0.004425	0.050192	--------
	2	1.168683	.000035	.118005	--------		2	.614530	.000001	.037009	--------
	3	.710806	.001536	.103657	--------		3	.492687	.000241	.023893	--------
	4	.186473	.018153	--------	--------		4	.363748	.002679	--------	--------
5	1	2.079867	0.000467	0.087035	--------	16	1	2.006028	0.001361	0.067202	--------
	2	1.138863	.000096	.107538	--------		2	.975008	.000109	.071023	--------
	3	.612887	.004015	.092907	--------		3	.629348	.003612	.058741	--------
	4	.187098	[a].047944	--------	--------		4	.253270	.043157	--------	--------
6	1	1.819665	0.001131	0.075089	--------	17	1	2.077556	0.000444	0.081940	--------
	2	.970001	.000184	.073694	--------		2	1.137234	.000101	.098870	--------
	3	.503652	.007068	.059677	--------		3	.660529	.003678	.085230	--------
	4	.216505	[a].086501	--------	--------		4	.203522	.043925	--------	--------
7	1	2.261596	0.000416	0.081356	--------	18	1	1.775590	0.000583	0.084939	0.000167
	2	1.197460	.000052	.104609	--------		2	1.043199	.000306	.089807	.000220
	3	.767999	.001659	.091547	--------		3	.499444	.010371	.073231	.004929
	4	.207937	.019639	--------	--------		4	.185184	.123151	--------	.057726
8	1	3.617377	0.000242	0.044272	--------	19	1	2.123732	0.000494	0.078944	0.000169
	2	1.978100	.000059	.052393	--------		2	1.179375	.000217	.092382	.000220
	3	1.283077	.001701	.045143	--------		3	.670403	.006605	.077559	.004995
	4	.389664	.020323	--------	--------		4	.207632	[a].074534	--------	.057726
9	1	2.327139	0.000385	0.074838	--------	20	1	2.318563	0.000410	0.071656	0.000132
	2	1.239180	.000057	.094290	--------		2	1.255749	.000149	.086199	.000172
	3	.849066	.001430	.082402	--------		3	.898098	.003581	.073309	.003933
	4	.231106	.016932	--------	--------		4	.243430	.038636	--------	.045196
10	1	1.988216	0.004347	0.052003	--------	21	1	2.376778	0.000452	0.065982	0.000302
	2	.622923	.000001	.040007	--------		2	1.300337	.000263	.077201	.000393
	3	.494339	.000281	.026852	--------		3	.973256	.006253	.063607	.008799
	4	.349836	.003151	--------	--------		4	.273858	.065979	--------	.102843
11	1	1.634896	0.000567	0.063980	--------						
	2	1.035557	.000369	.044880	--------						
	3	.439890	.011889	.031834	--------						
	4	.235532	.159501	--------	--------						

[a] Σ_A Σ_p, corrected for fast absorption, of 0.09717 was added to these values.

TABLE III. - LETHARGY GROUP STRUCTURE USED IN 71-GROUP ONE-DIMENSIONAL CALCULATION

[Zero lethargy is defined as 10 Mev.]

Group	Lethargy breakpoint	Energy breakpoint	Group	Lethargy breakpoint	Energy breakpoint
1	0.25	7.79 Mev	37	9.25	0.961 Kev
2	.50	6.07	38	9.50	.749
3	.75	4.72	39	9.75	.583
4	1.00	3.68	40	10.00	.454
5	1.25	2.87	41	10.25	.354
6	1.50	2.23	42	10.50	.275
7	1.75	1.74	43	10.75	.215
8	2.00	1.35	44	11.00	.167
9	2.25	1.05	45	11.25	.130
10	2.50	.821	46	11.50	.101
11	2.75	.639	47	11.75	78.9 ev
12	3.00	.498	48	12.00	61.4
13	3.25	.388	49	12.25	47.9
14	3.50	.302	50	12.50	37.3
15	3.75	.235	51	12.75	29.0
16	4.00	.183	52	13.00	22.6
17	4.25	.143	53	13.25	17.6
18	4.50	.111	54	13.50	13.7
19	4.75	86.5 Kev	55	13.75	10.7
20	5.00	67.4	56	14.00	8.32
21	5.25	52.5	57	14.25	6.48
22	5.50	40.9	58	14.50	5.04
23	5.75	31.8	59	14.76	3.88
24	6.00	24.8	60	15.00	3.06
25	6.25	19.3	61	15.26	2.35
26	6.50	15.0	62	15.50	1.86
27	6.75	11.7	63	15.76	1.43
28	7.00	9.12	64	16.00	1.13
29	7.25	7.10	65	16.30	.827
30*	7.50	5.53	66	16.60	.611
31	7.75	4.31	67	17.00	.410
32	8.00	3.36	68	17.30	.305
33	8.25	2.61	69	17.60	.224
34	8.50	2.04	70	18.2	.125
35	8.75	1.59	71	19.8	.0253
36	9.00	1.23		(thermal spike)	

TABLE IV. - LIMITS OF FLUX VARIATION AT SEVERAL EXPERIMENTAL LOCATIONS

[These values have been taken from the vertical calculation having shim rods at 15.35 in. and the "rods out" calculation containing boron. The fluxes shown have been normalized to 60 mw and are spatial averages over the fueled core length in the east-west dimension.]

Position	Indicated shim bank height, in.	Neutron flux (i^{th} group)			
		φ_1, >0.821 Mev	φ_2, 0.821 Mev to 5.5 kev	φ_3, 5.5 kev to 0.125 ev	φ_4, <0.125 ev
Axis of HT-1	[a]15.35	1.5×10^{13}	1.8×10^{13}	2.5×10^{13}	2.4×10^{14}
	[a]30.90	1.3×10^{13}	1.5×10^{13}	2.3×10^{13}	2.2×10^{14}
Axis of HT-2	15.35	1.9×10^{12}	2.2×10^{12}	3.2×10^{12}	3.3×10^{13}
	30.90	1.5×10^{12}	1.7×10^{12}	2.5×10^{12}	2.7×10^{13}
Center of LA row at elevation of core horizontal midplane	15.35	1.7×10^{14}	2.5×10^{14}	3.2×10^{14}	7.9×10^{14}
	30.90	1.9×10^{14}	2.9×10^{14}	3.7×10^{14}	8.5×10^{14}
Center of RA row 3 in. from top of reflector grid	15.35	1.3×10^{13}	2.3×10^{13}	3.8×10^{13}	1.7×10^{14}
	30.90	2.9×10^{13}	5.2×10^{13}	8.8×10^{13}	3.6×10^{14}
Center of RB row 3 in. from top of reflector grid	15.35	2.3×10^{12}	4.7×10^{12}	1.0×10^{13}	9.2×10^{13}
	30.90	5.0×10^{12}	1.1×10^{13}	2.3×10^{13}	1.8×10^{14}
Center of RC row 3 in. from top of reflector grid	15.35	4.0×10^{11}	8.8×10^{11}	2.2×10^{12}	3.5×10^{13}
	30.90	8.0×10^{11}	1.8×10^{12}	4.4×10^{12}	6.5×10^{13}
Center of RD row at elevation of core horizontal midplane	15.35	1.6×10^{11}	3.1×10^{11}	7.0×10^{11}	2.4×10^{13}
	30.90	1.7×10^{11}	3.4×10^{11}	7.7×10^{11}	2.6×10^{13}
$1\frac{1}{2}$ in. north of LA row in water at elevation of HB-1	15.35	9.4×10^{12}	1.2×10^{13}	1.8×10^{13}	1.6×10^{14}
	30.90	1.7×10^{13}	2.1×10^{13}	3.3×10^{13}	2.6×10^{14}
$1\frac{1}{2}$ in. south of reflector lattice in water at elevation of HB-4	15.35	2.7×10^{10}	3.7×10^{10}	7.1×10^{10}	4.1×10^{12}
	30.90	2.0×10^{10}	2.7×10^{10}	5.3×10^{10}	3.0×10^{12}
$1\frac{1}{2}$ in. south of reflector lattice in water at elevation of HB-6	15.35	1.0×10^{10}	1.4×10^{10}	2.9×10^{10}	1.7×10^{12}
	30.90	1.9×10^{10}	2.6×10^{10}	5.3×10^{10}	2.9×10^{12}

[a]15.35 corresponds to clean critical; 30.90 denotes end of life.

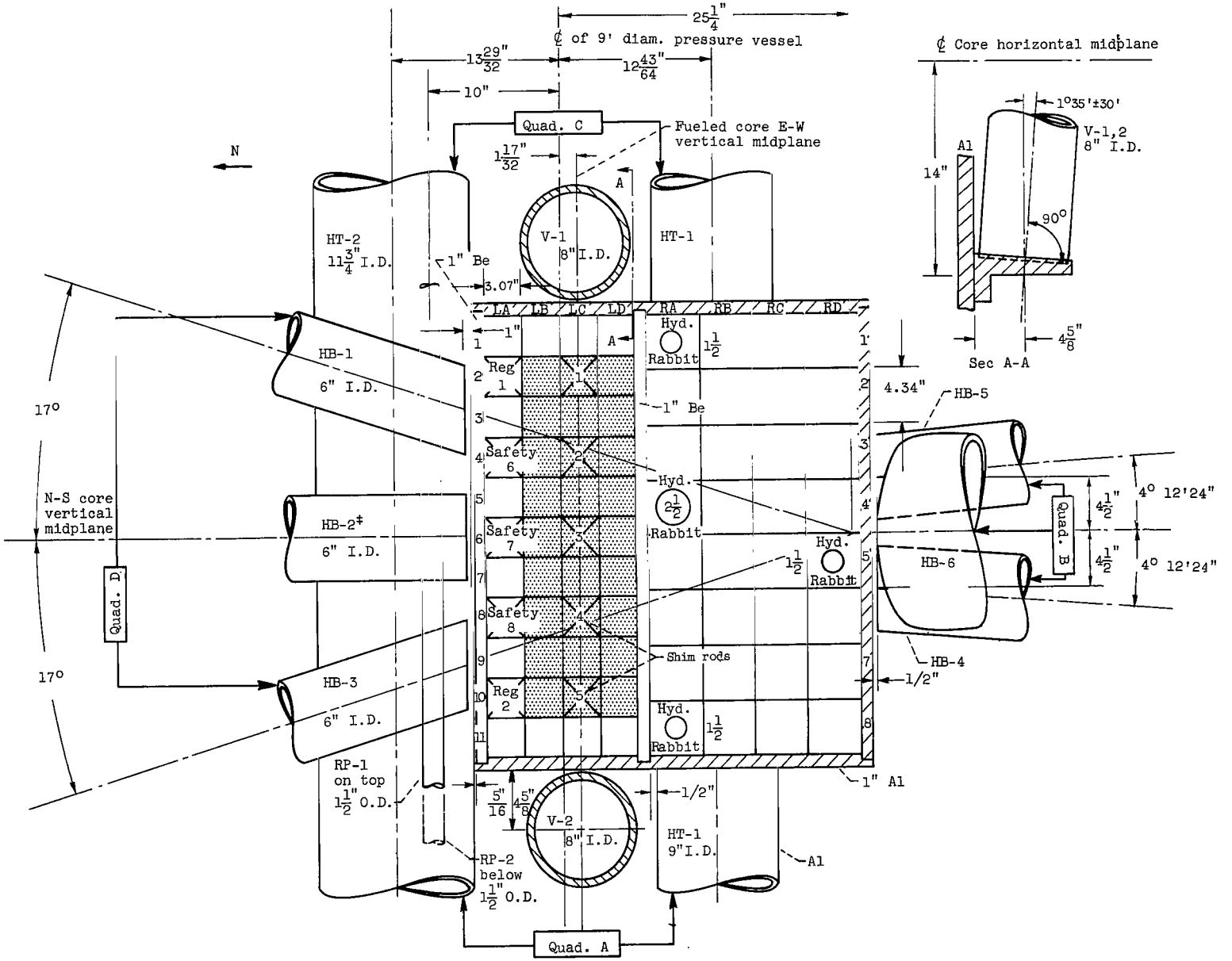

Figure 1. - Horizontal plan view of Plum Brook Reactor core, reflectors, and experimental test holes.

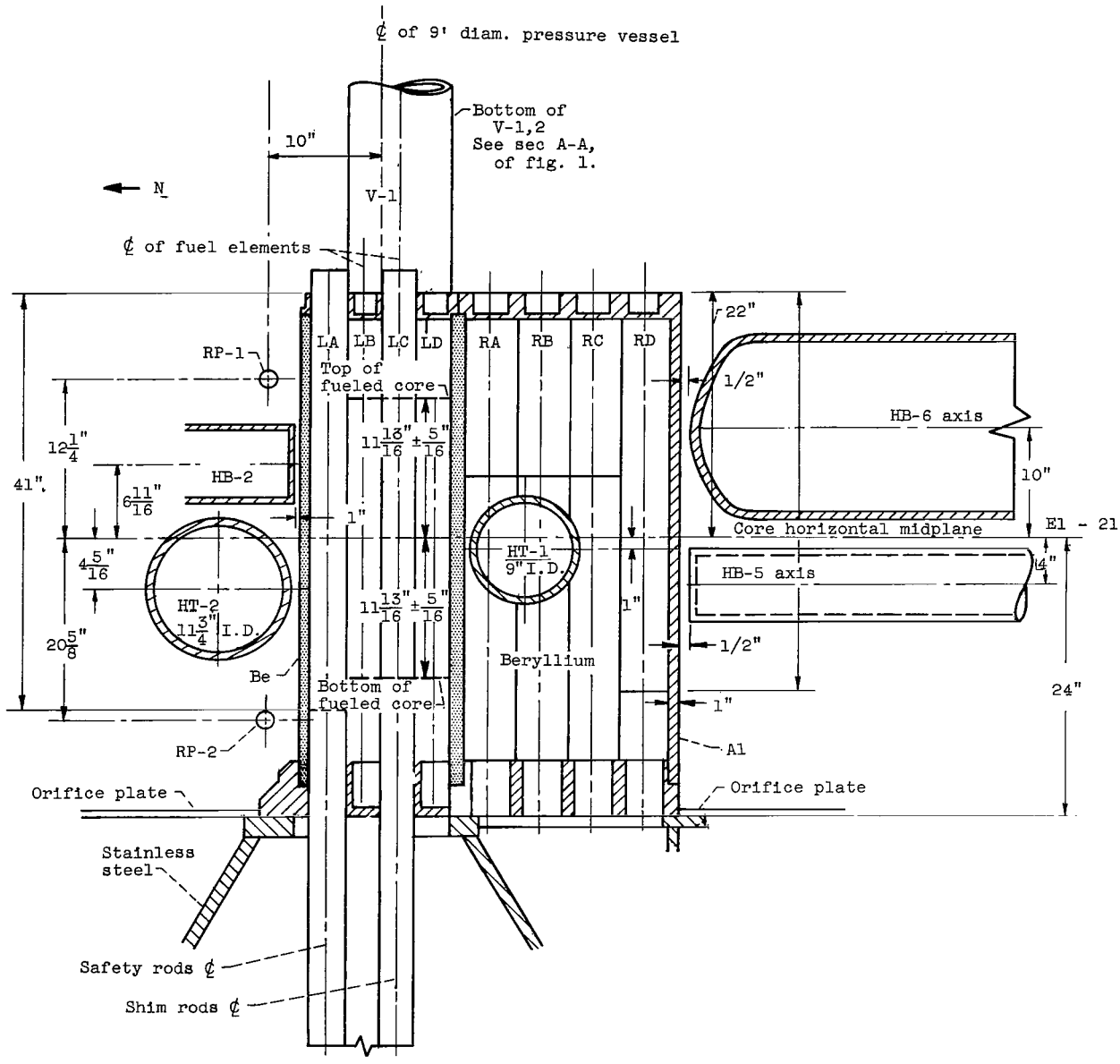

Figure 2. - Vertical section of Plum Brook Reactor core, reflectors, and experimental test holes (cutaway at N-S core vertical midplane).

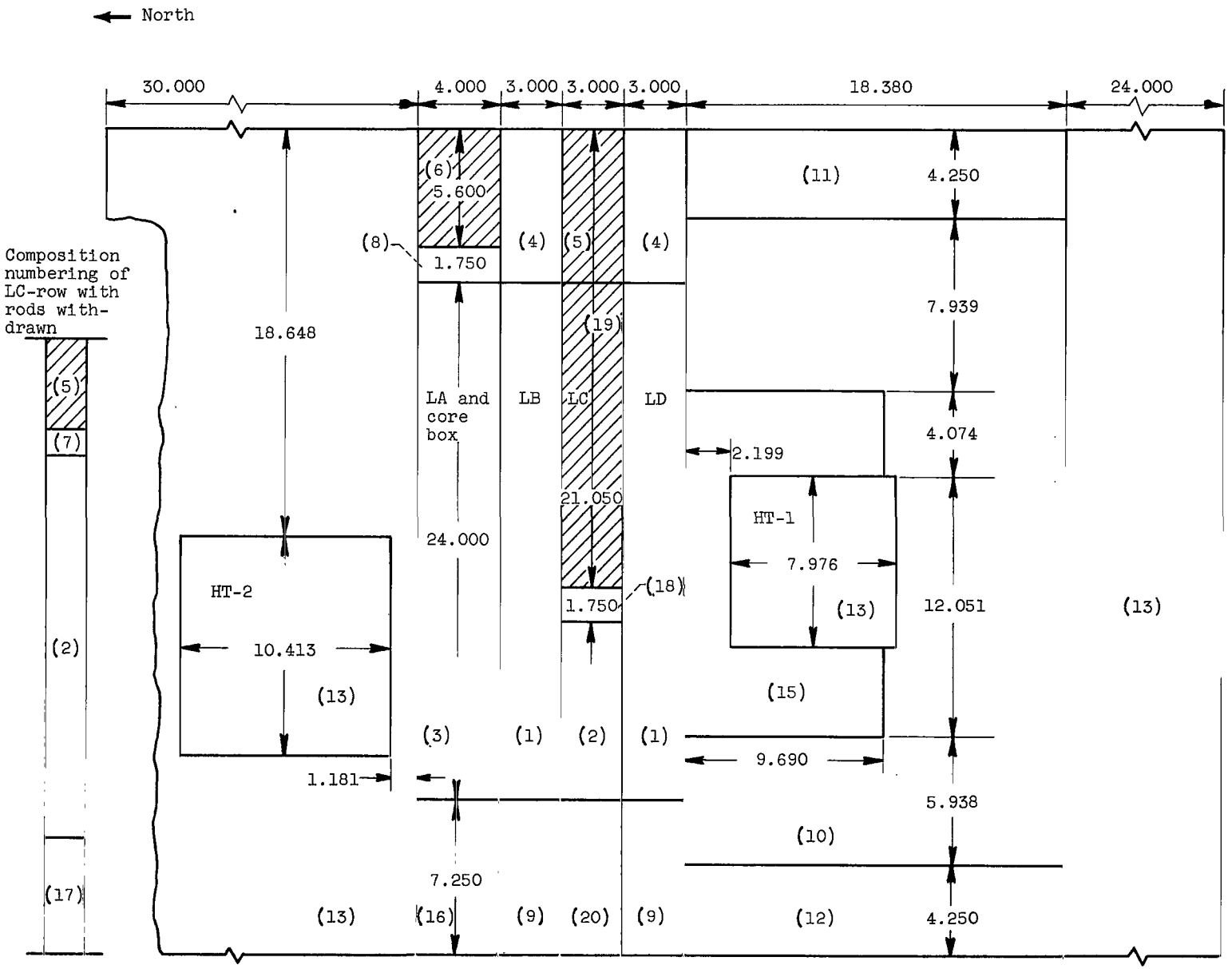

Figure 3. - Geometrical layout of vertical plane calculations. All dimensions are given in inches; (x) denotes material composition; shaded areas denote presence of rods.

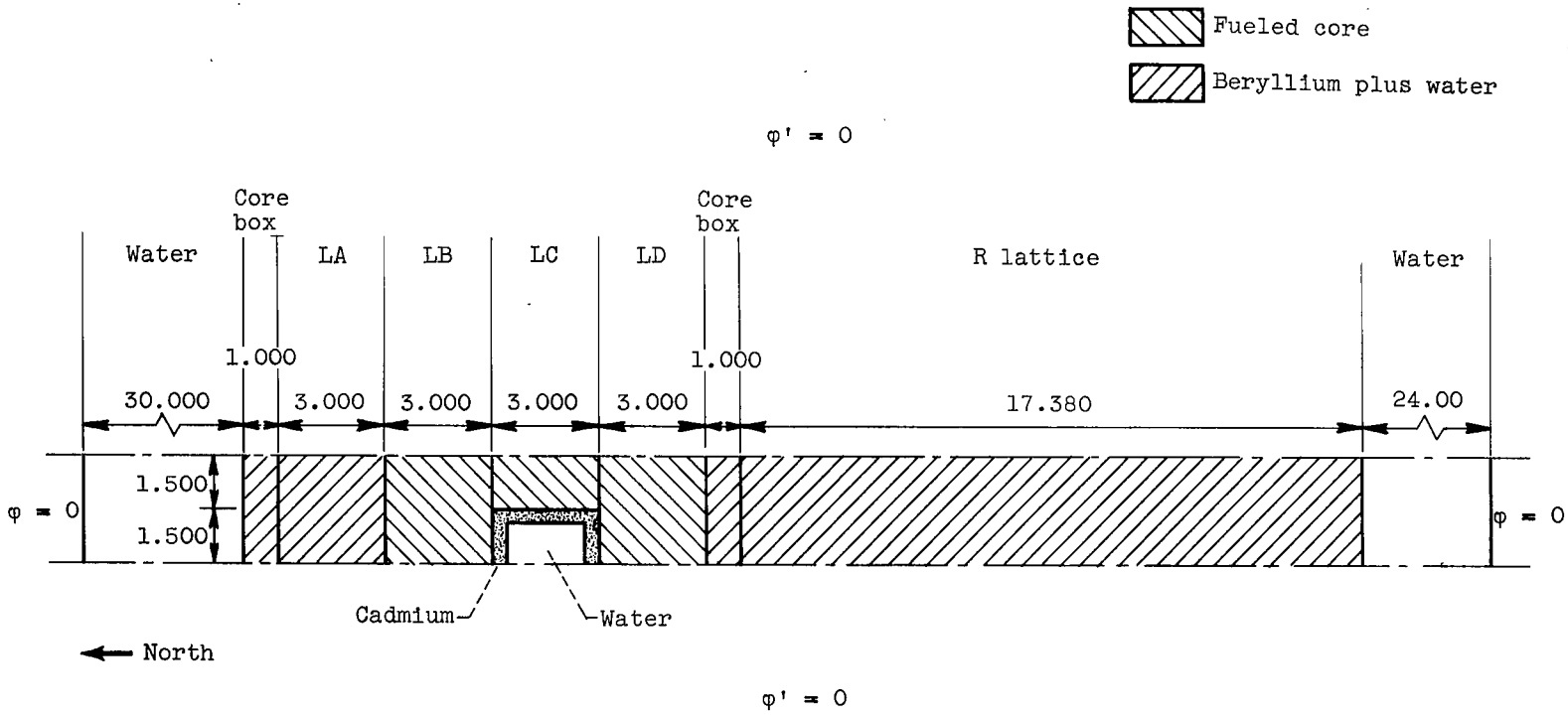

Figure 4. - Cell representation of core and reflectors. All dimensions are in inches.

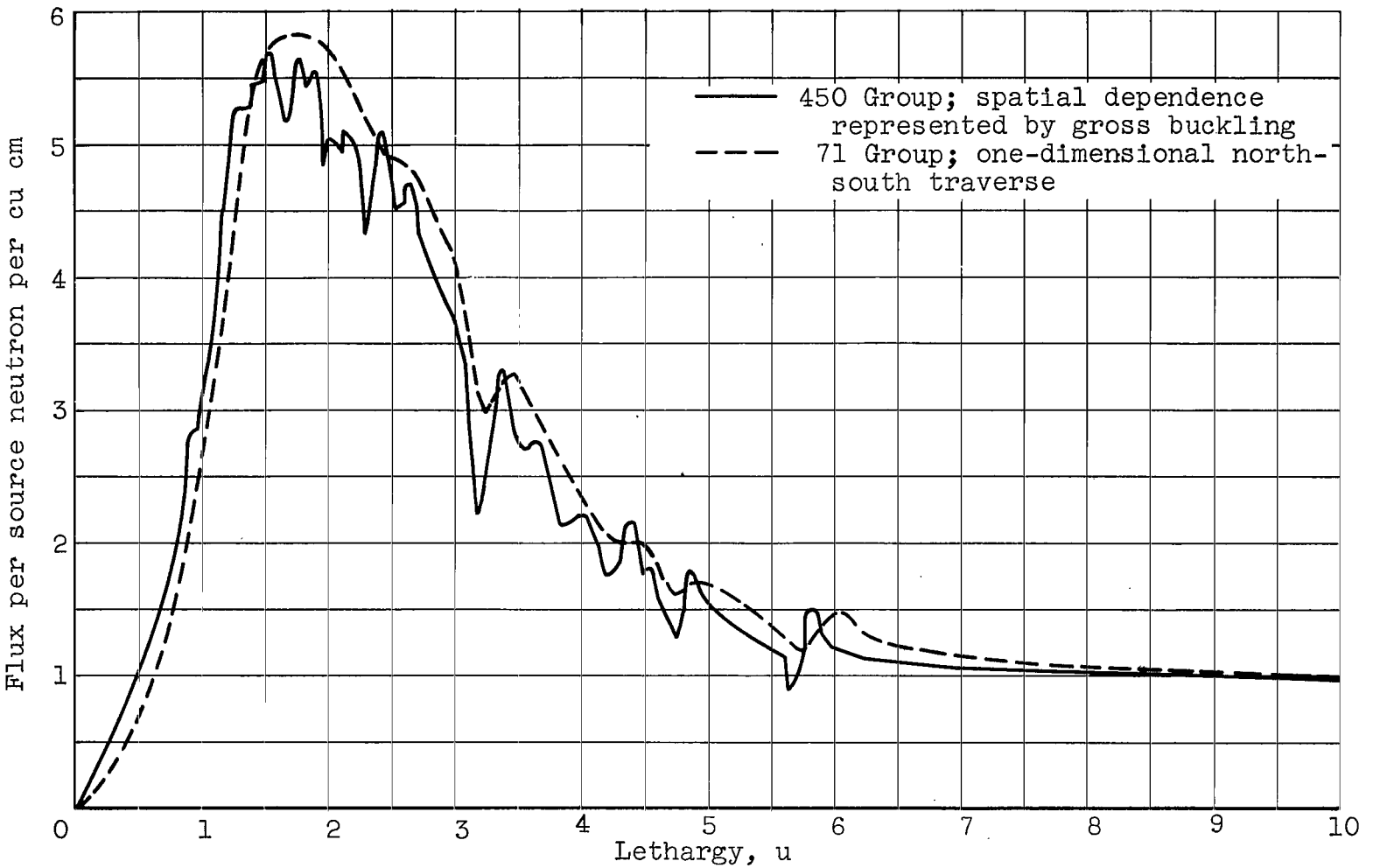

Figure 5. - Comparison of 450-group to 71-group flux solutions for fueled core material. Normalized to 60 megawatts, 4.806×10^{13}.

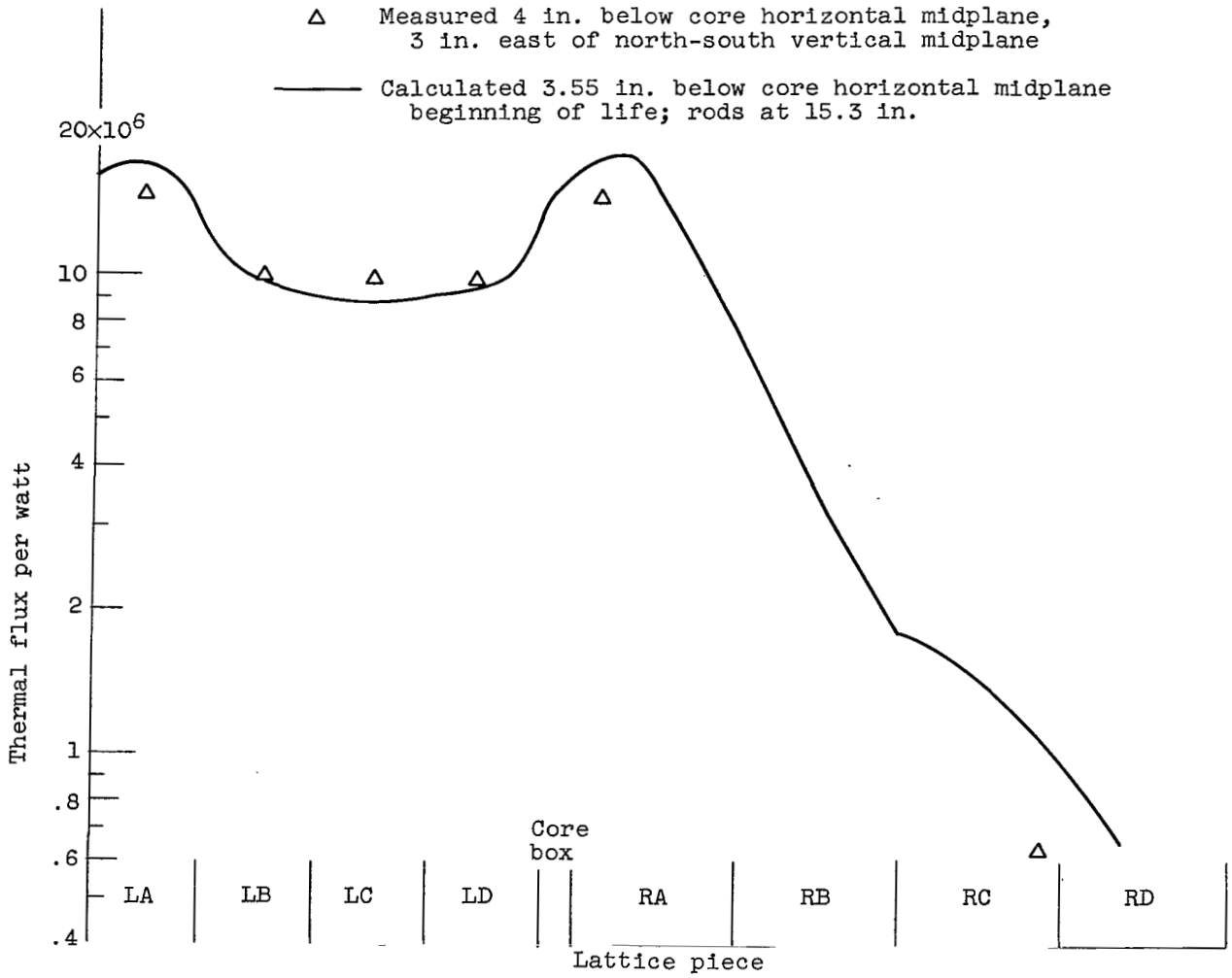

Figure 6. - Comparison of measured and calculated thermal flux. North-south traverse; calculated flux depression due to water filled through hole; experimental uncertainty is ±20 percent at 90-percent confidence.

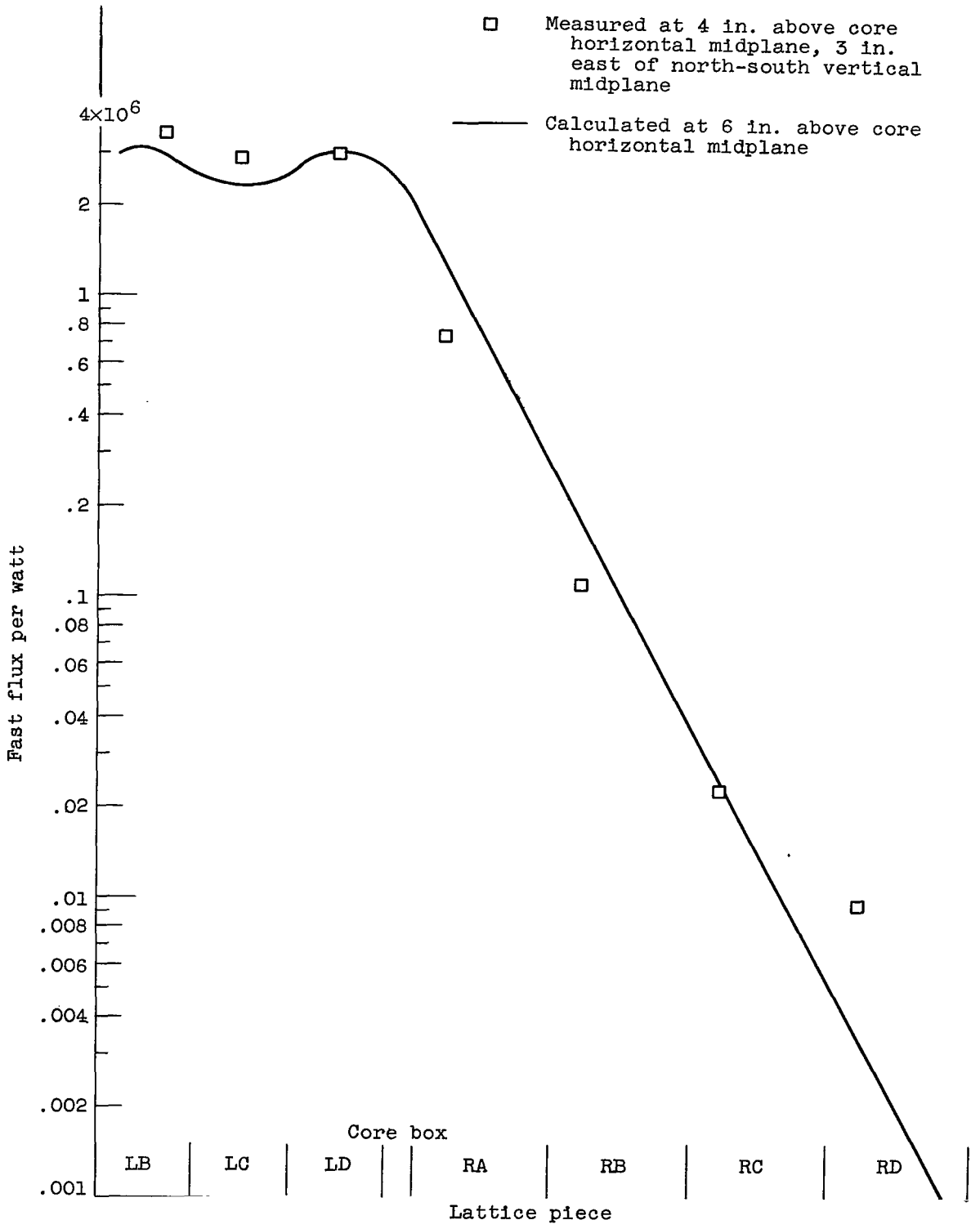

Figure 7. - Comparison of measured and calculated fast flux (>0.821 Mev); north-south traverse.

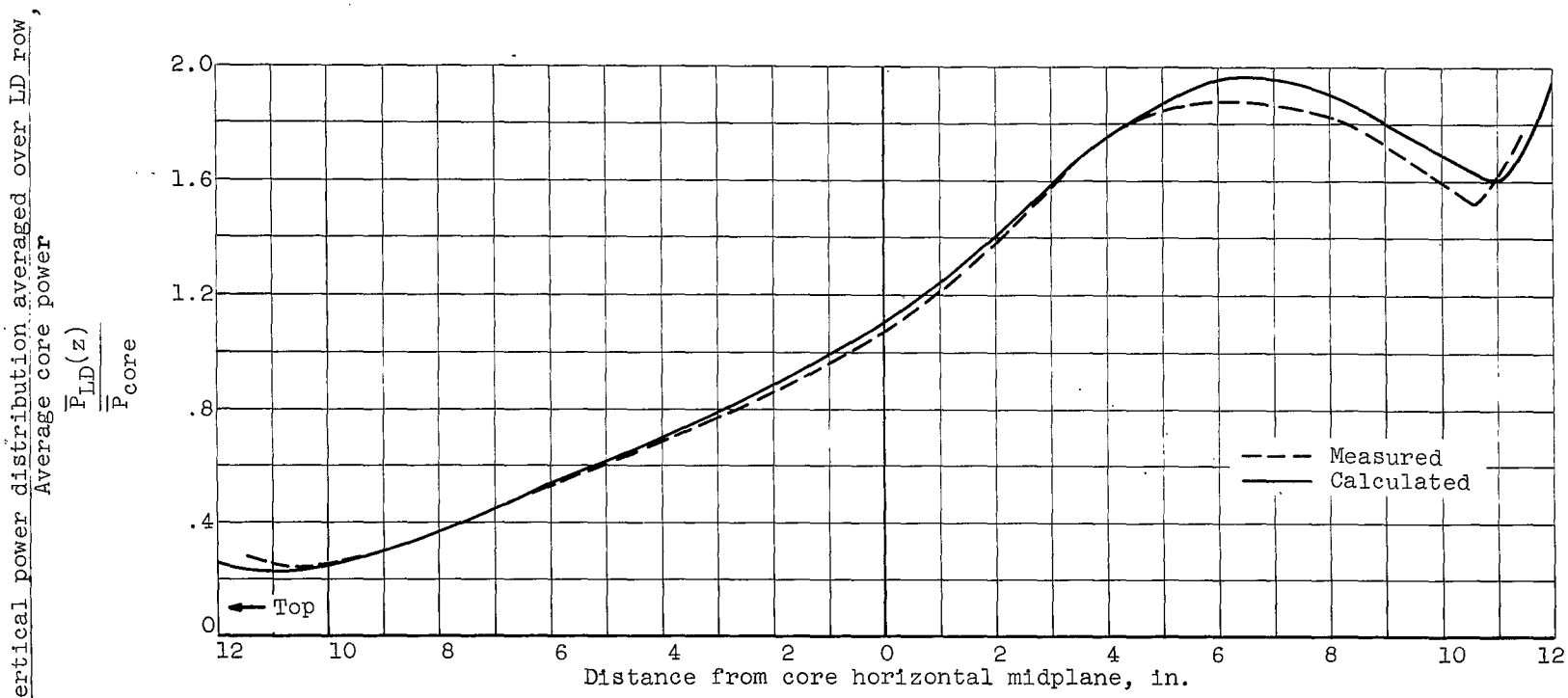

Figure 8. - Comparison of measured and calculated vertical power distribution in LD row.

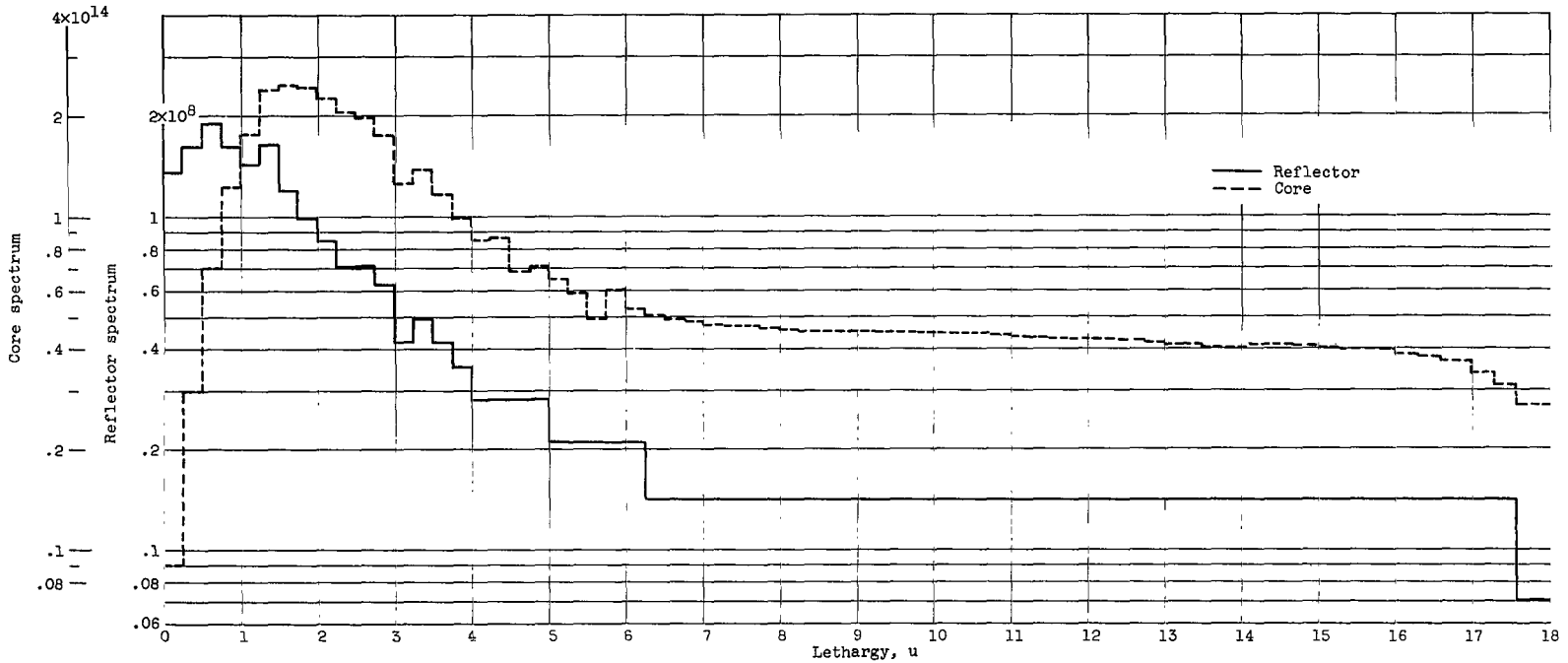

Figure 9. - Lethargy flux spectrum at 32.5 inches north of fueled core vertical midplane. Normalized to 60 megawatts of reactor power.

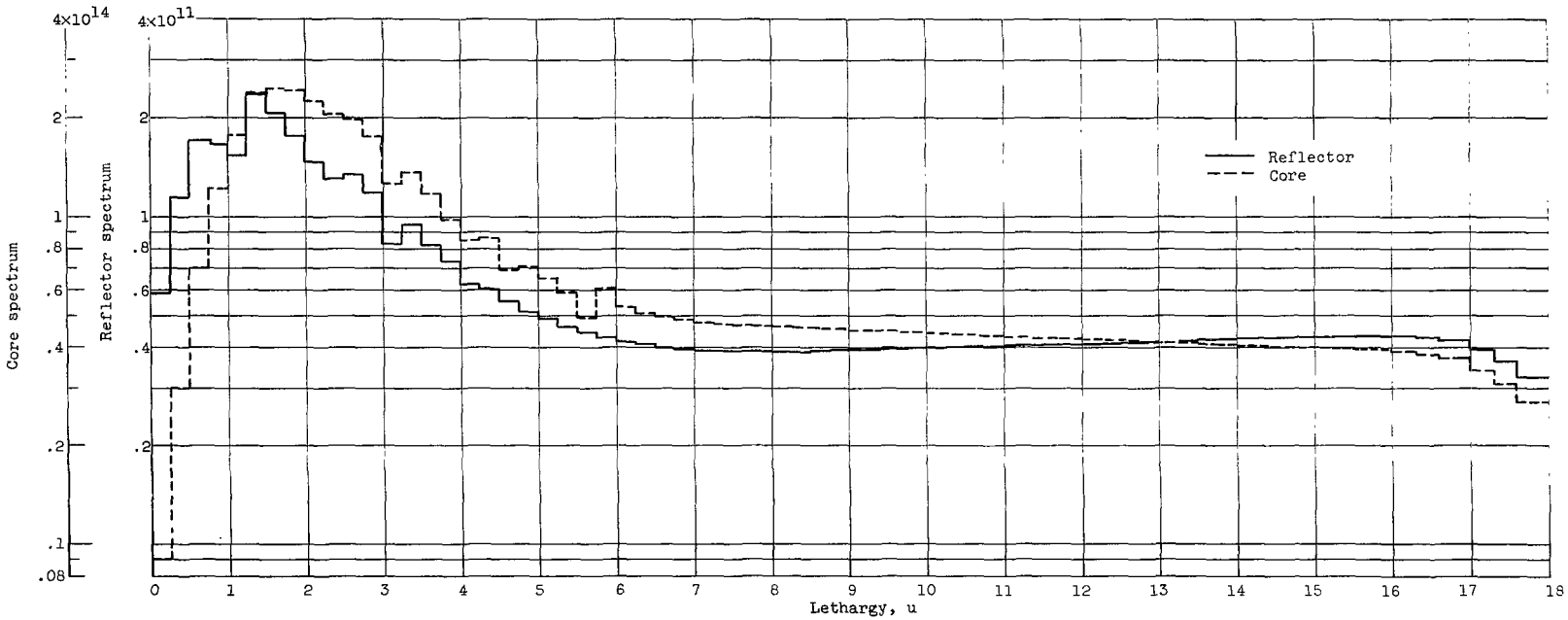

Figure 10. - Lethargy flux spectrum at 16.5 inches north of fueled core vertical midplane. Normalized to 60 megawatts of reactor power.

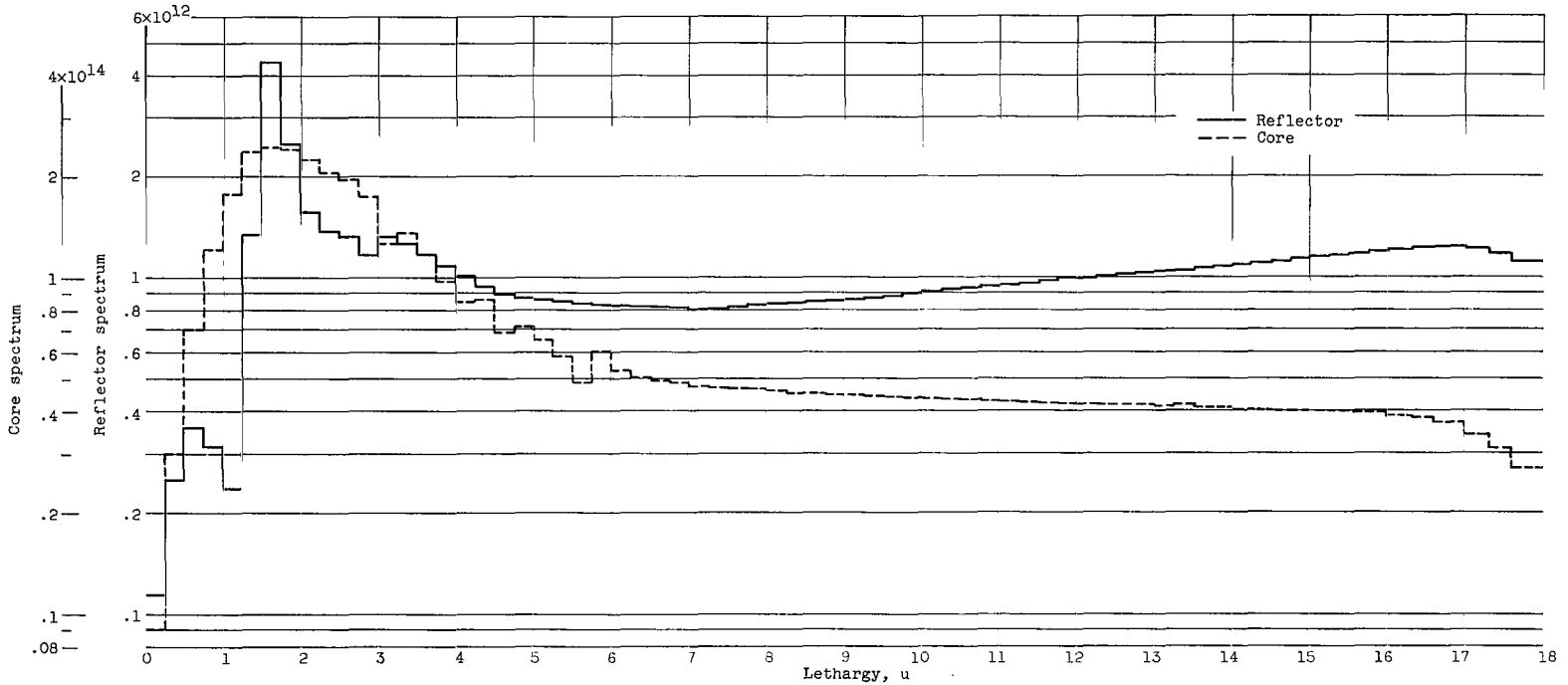

Figure 11. - Lethargy flux spectrum at 15.1 inches south of fueled core vertical midplane. Normalized to 60 megawatts of reactor power.

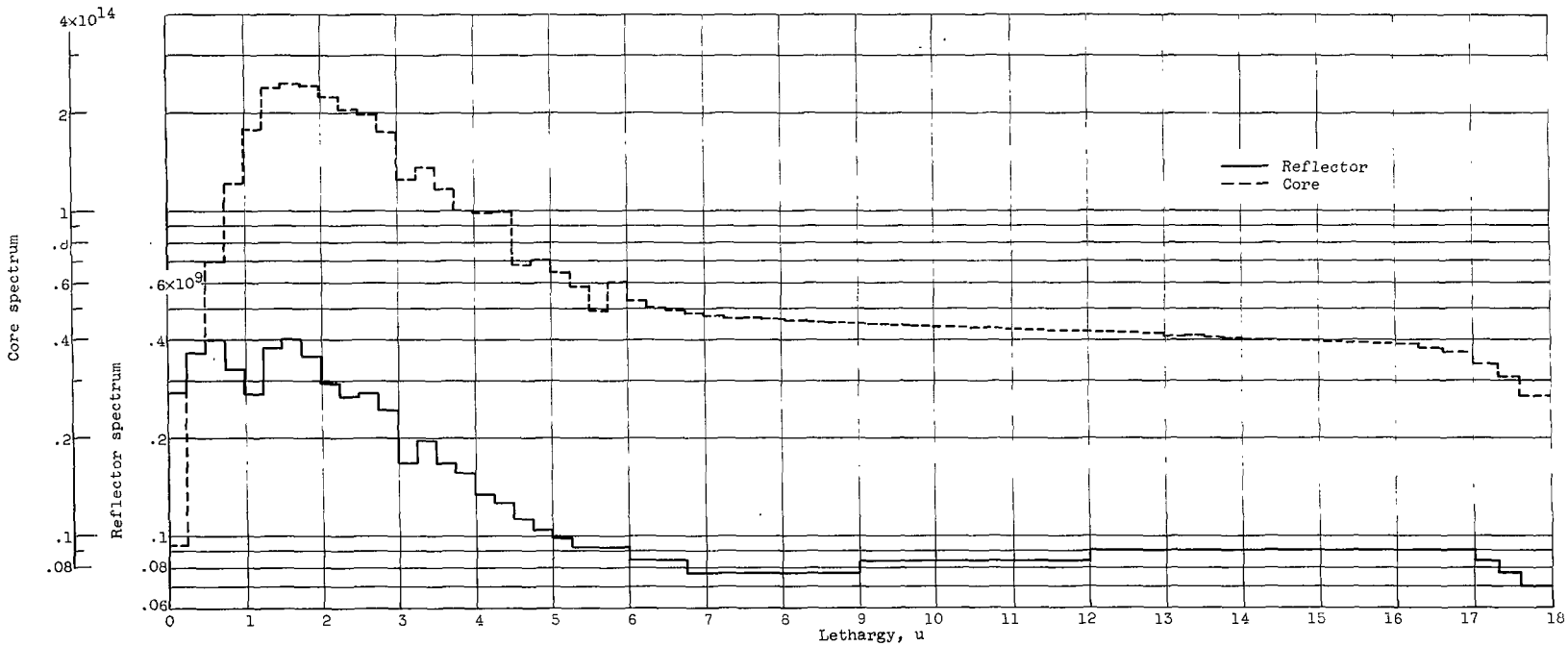

Figure 12. - Lethargy flux spectrum at 30.9 inches south of fueled core vertical midplane. Normalized to 60 megawatts of reactor power.

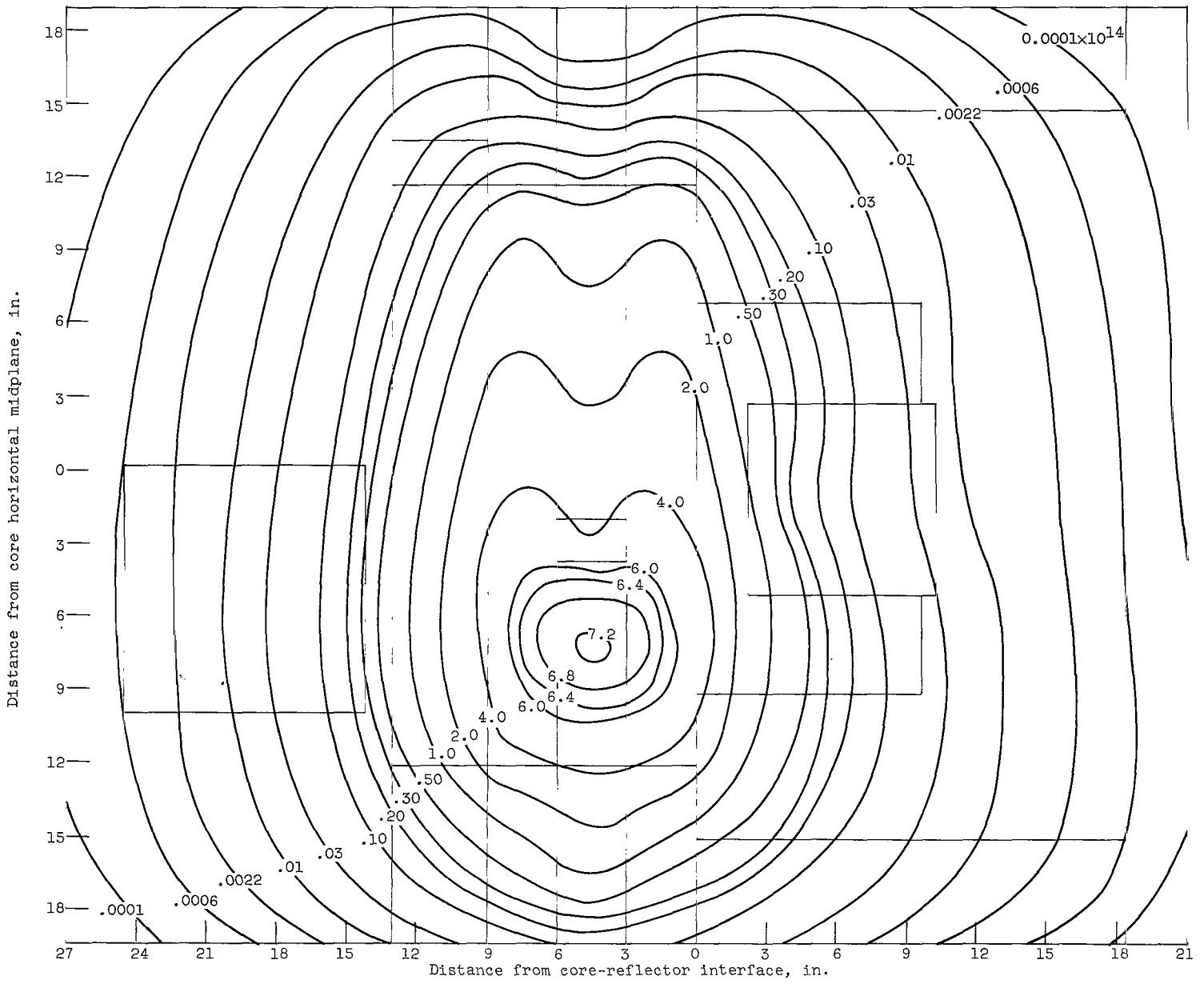

Figure 13. - Vertical calculation of group 1 flux distribution. Normalized to 60 megawatts of core power; control rods at 15.3 inches.

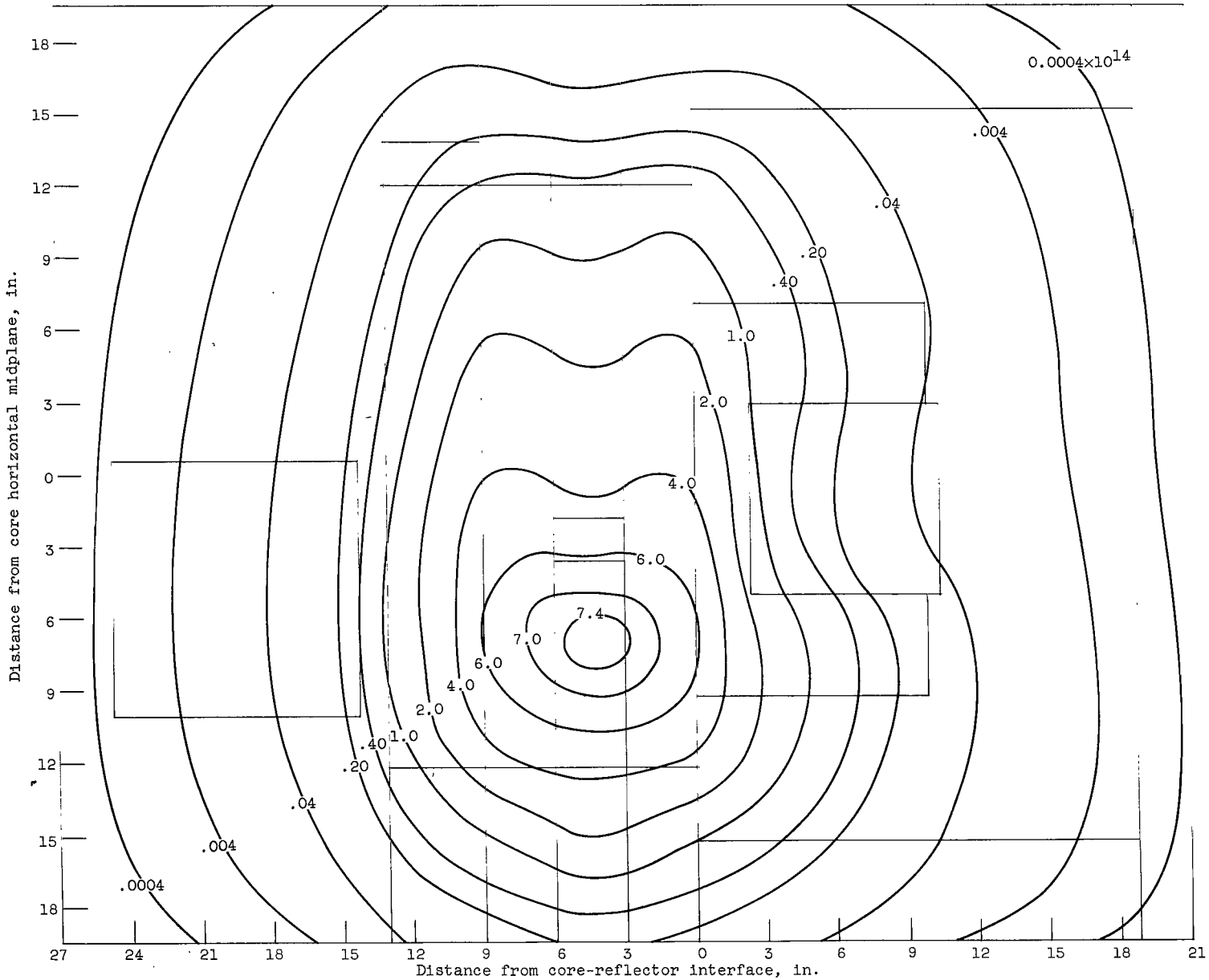

Figure 14. - Vertical calculation of group 2 flux distribution. Normalized to 60 megawatts of core power; control rods at 15.3 inches.

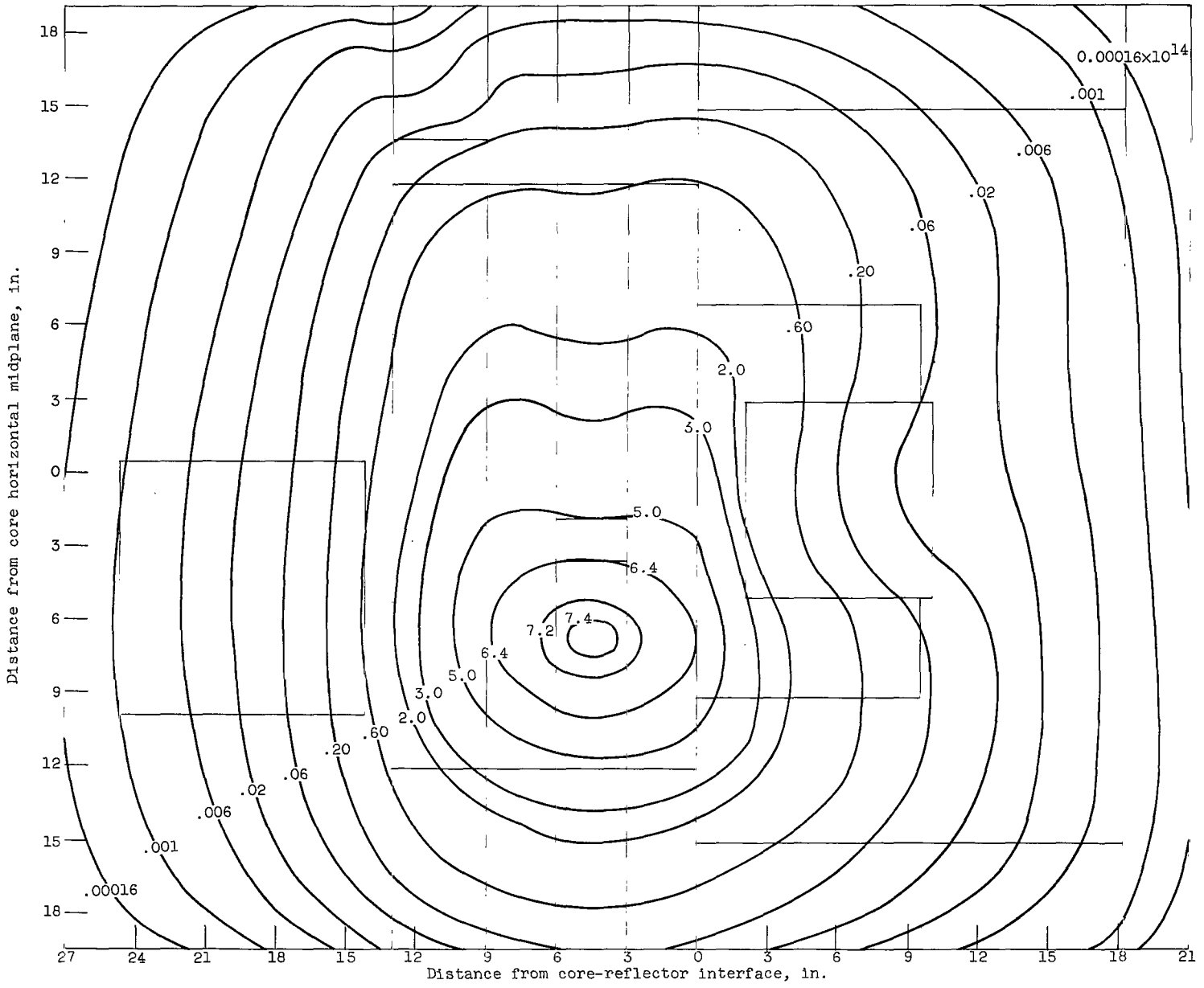

Figure 15. - Vertical calculation of group 3 flux distribution. Normalized to 60 megawatts of core power; control rods at 15.3 inches.

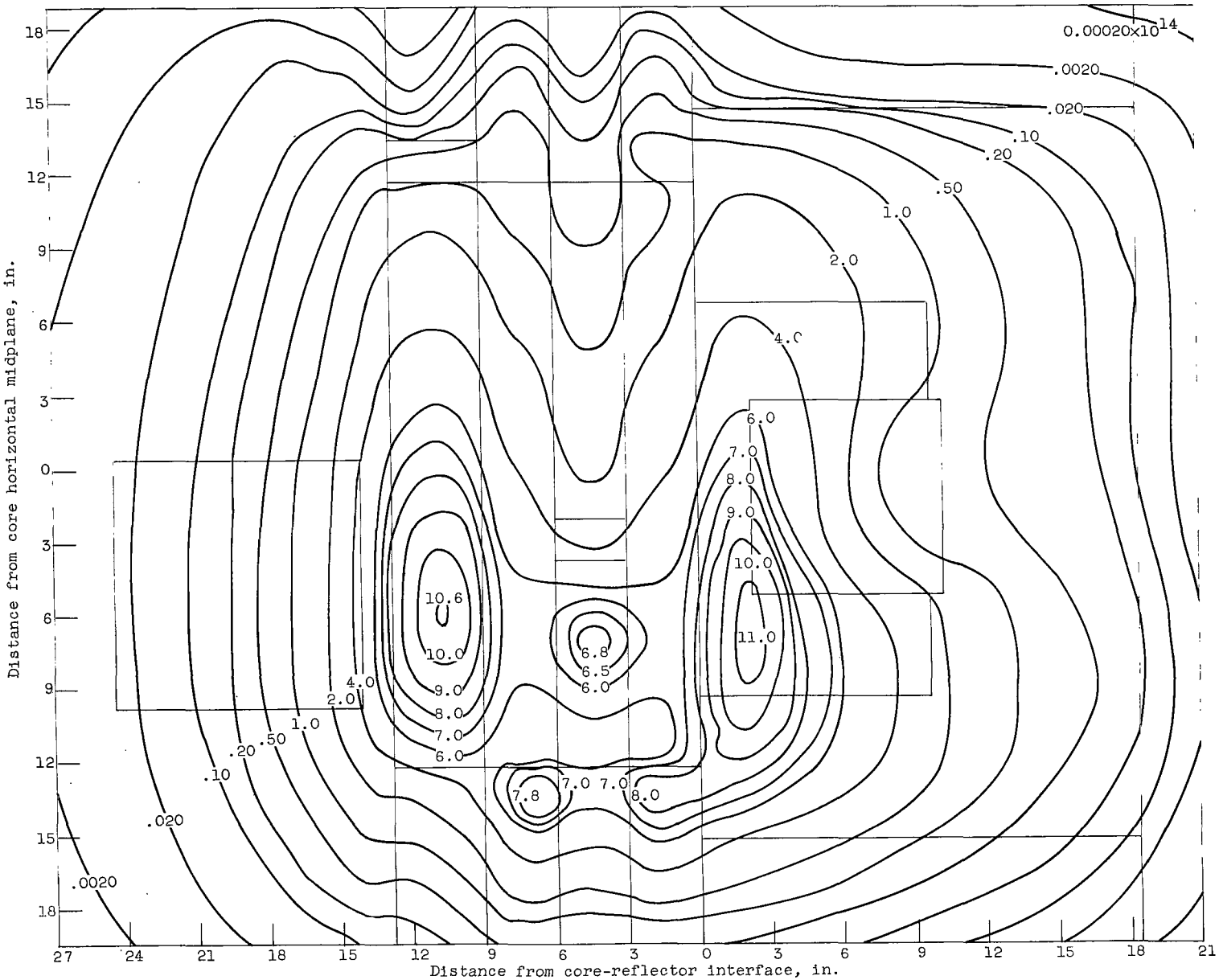

Figure 16. - Vertical calculation of thermal flux distribution. Normalized to 60 megawatts of core power; control rods at 15.3 inches.

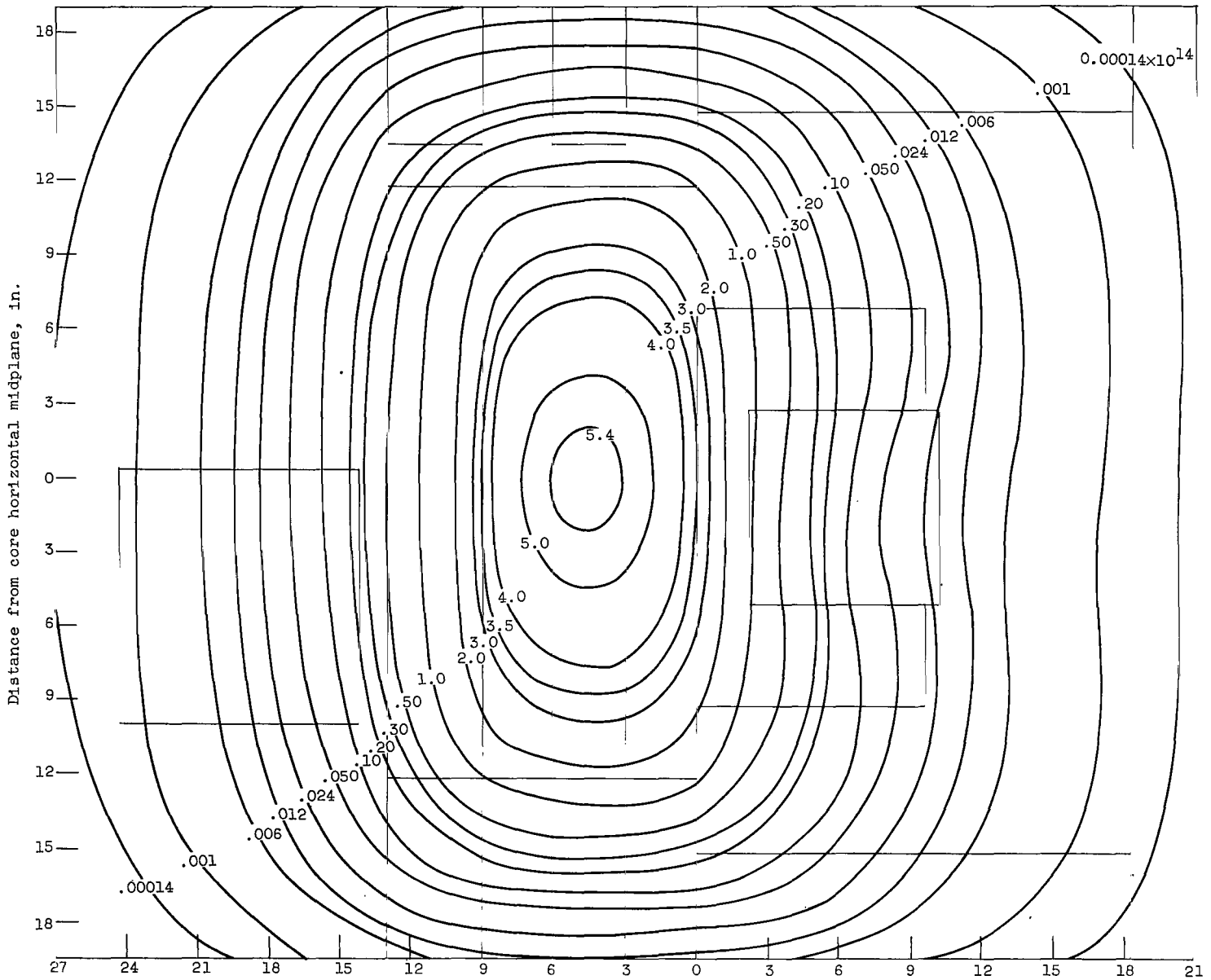

Figure 17. - Vertical calculation of group 1 flux distribution. Normalized to 60 megawatts of core power; control rods out.

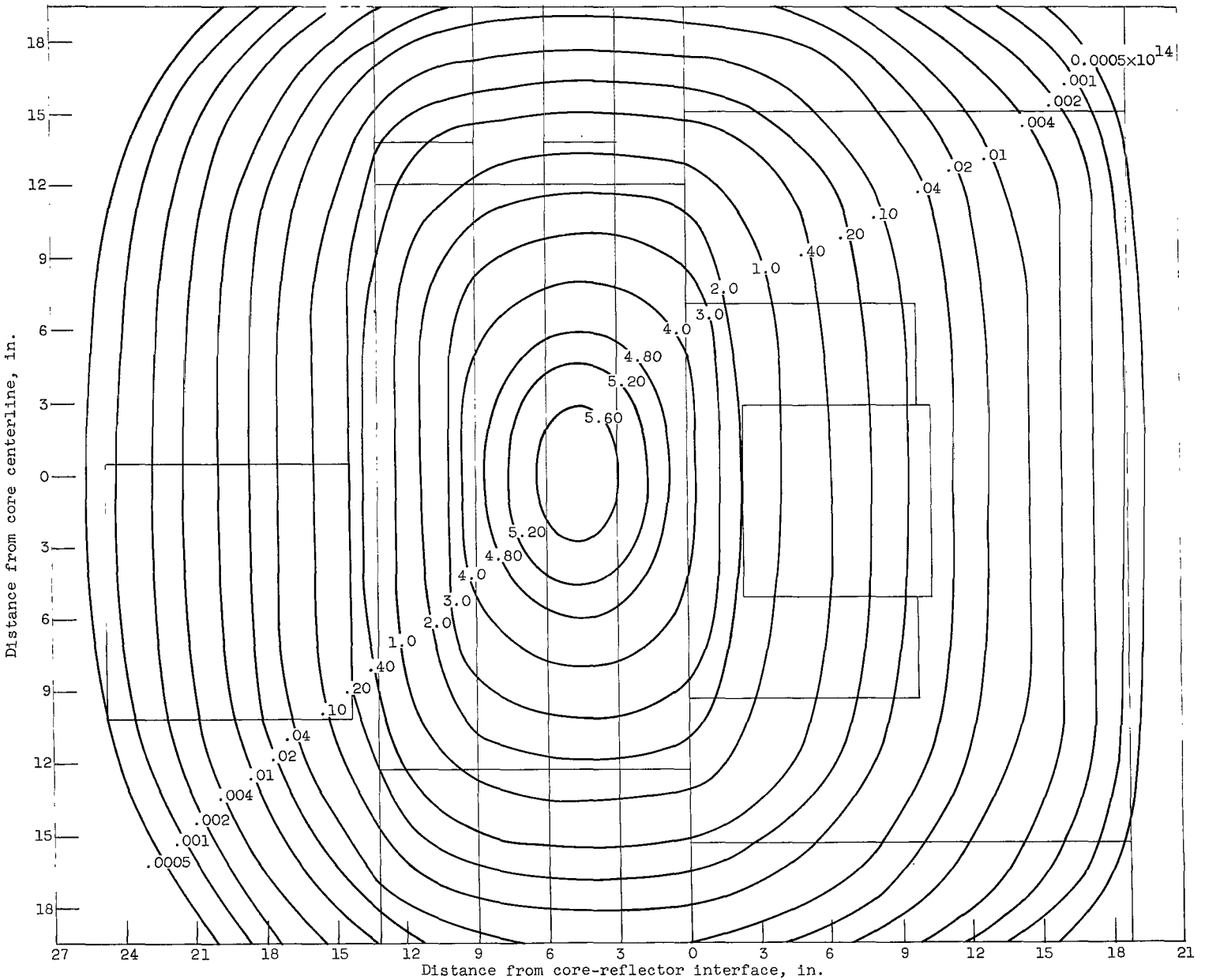

Figure 18. - Vertical calculation of group 2 flux distribution. Normalized to 60 megawatts of reactor power; control rods out.

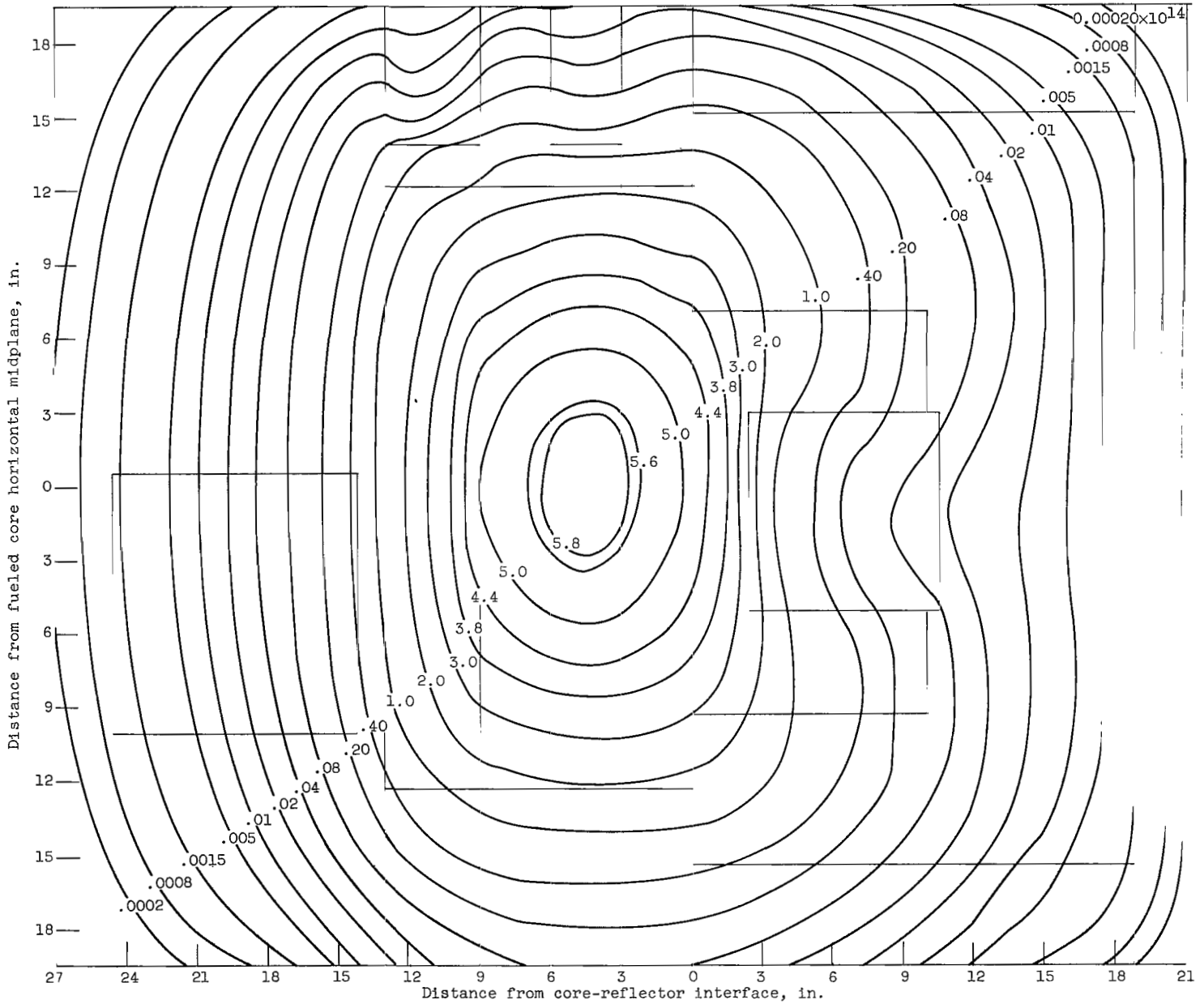

Figure 19. - Vertical calculation of group 3 flux distribution. Normalized to 60 megawatts of reactor power; control rods out.

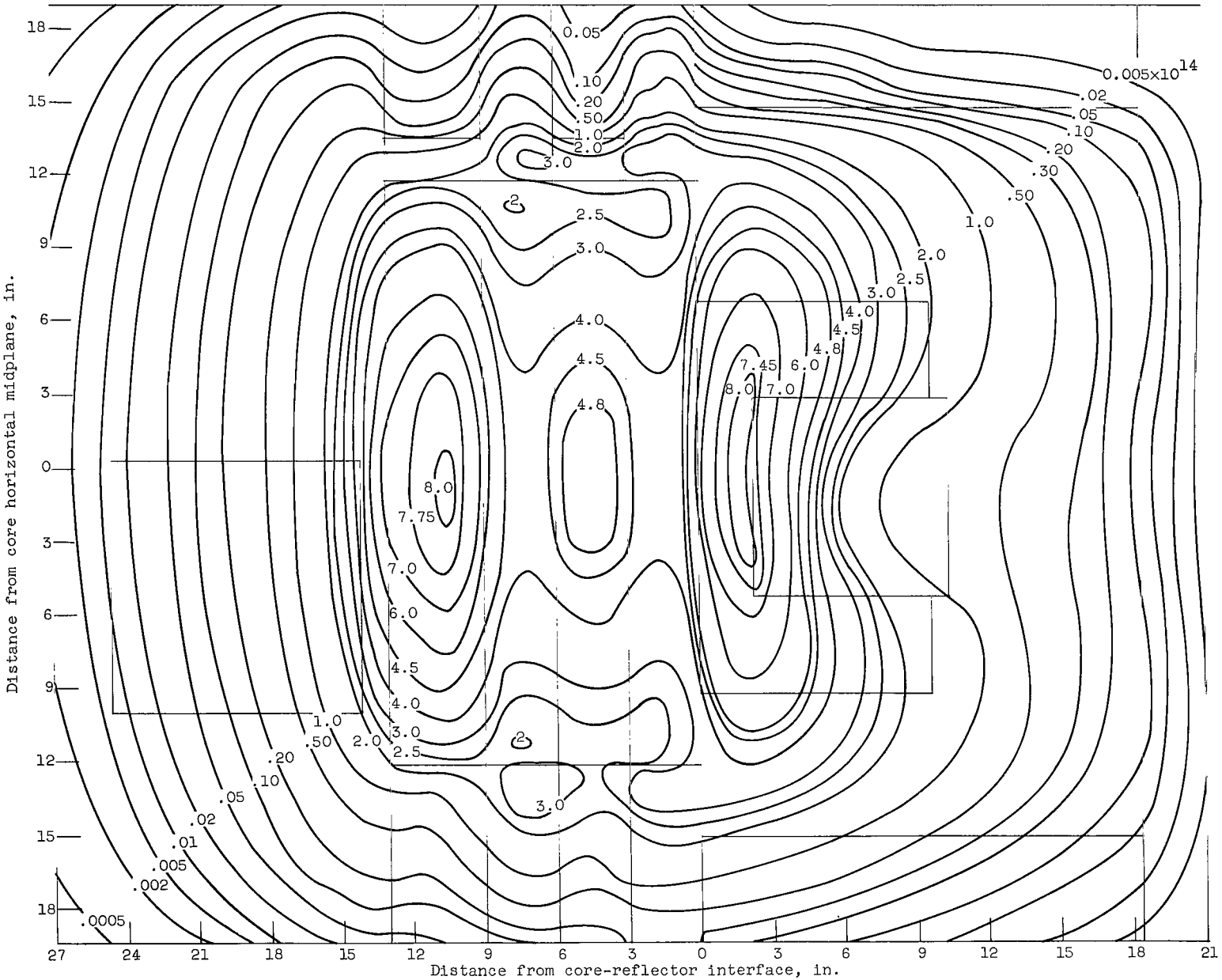

Figure 20. - Vertical calculation of thermal flux distribution. Normalized to 60 megawatts of core power; control rods out.

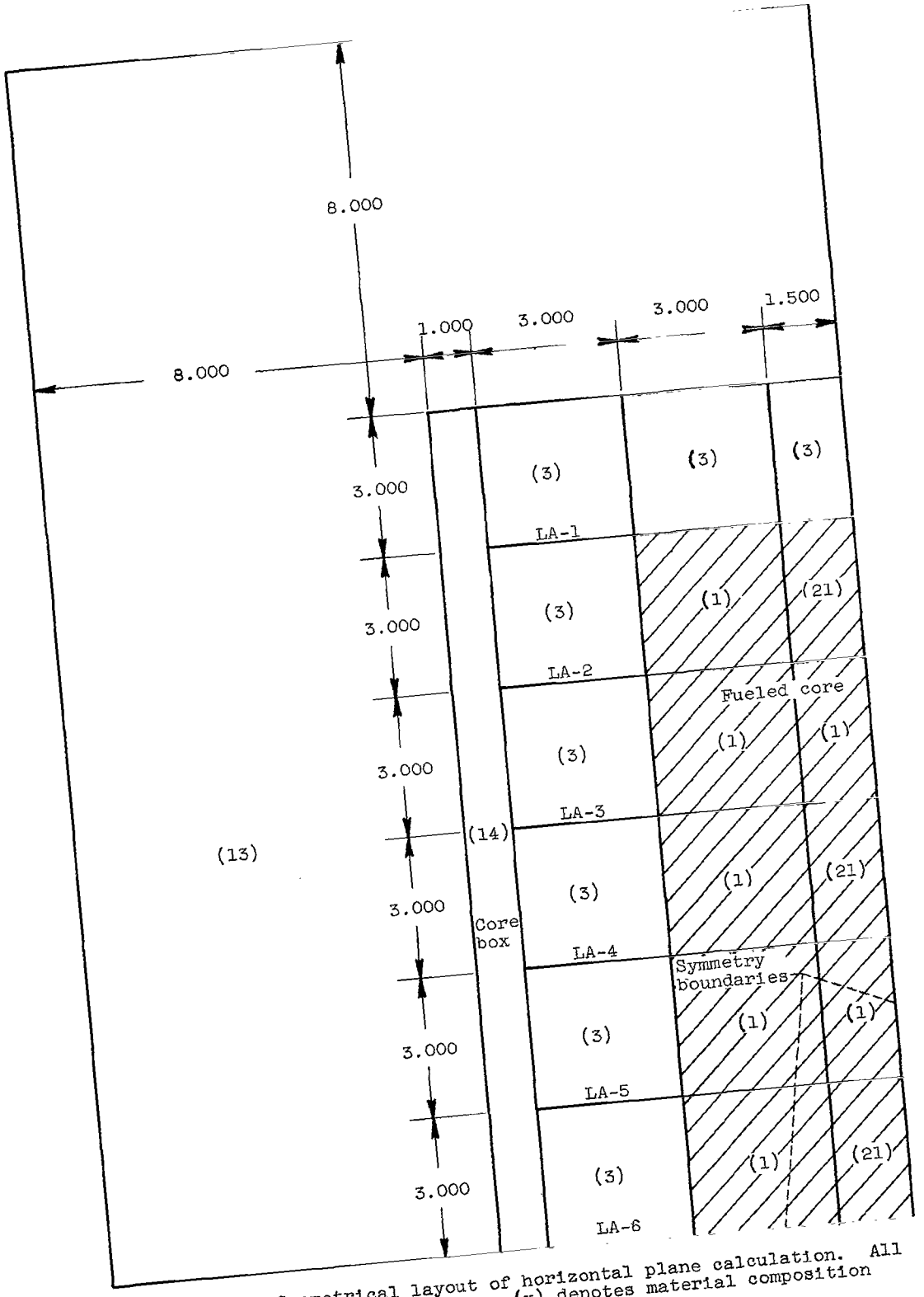

Figure 21. - Geometrical layout of horizontal plane calculation. All dimensions are given in inches; (x) denotes material composition corresponding to tables I and II.

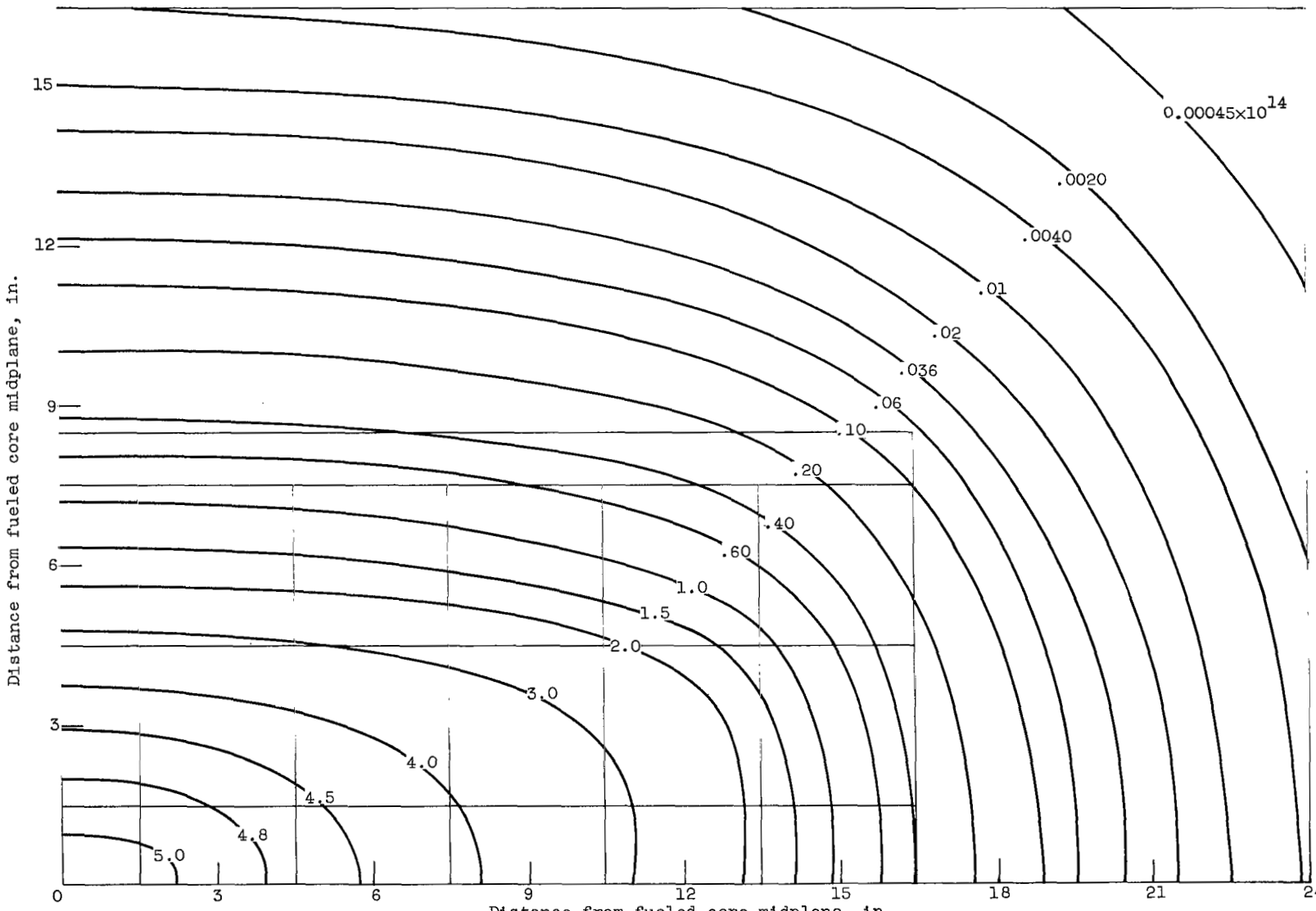

Figure 22. - Horizontal calculation of group 1 flux. Normalized to 60 megawatts of core power.

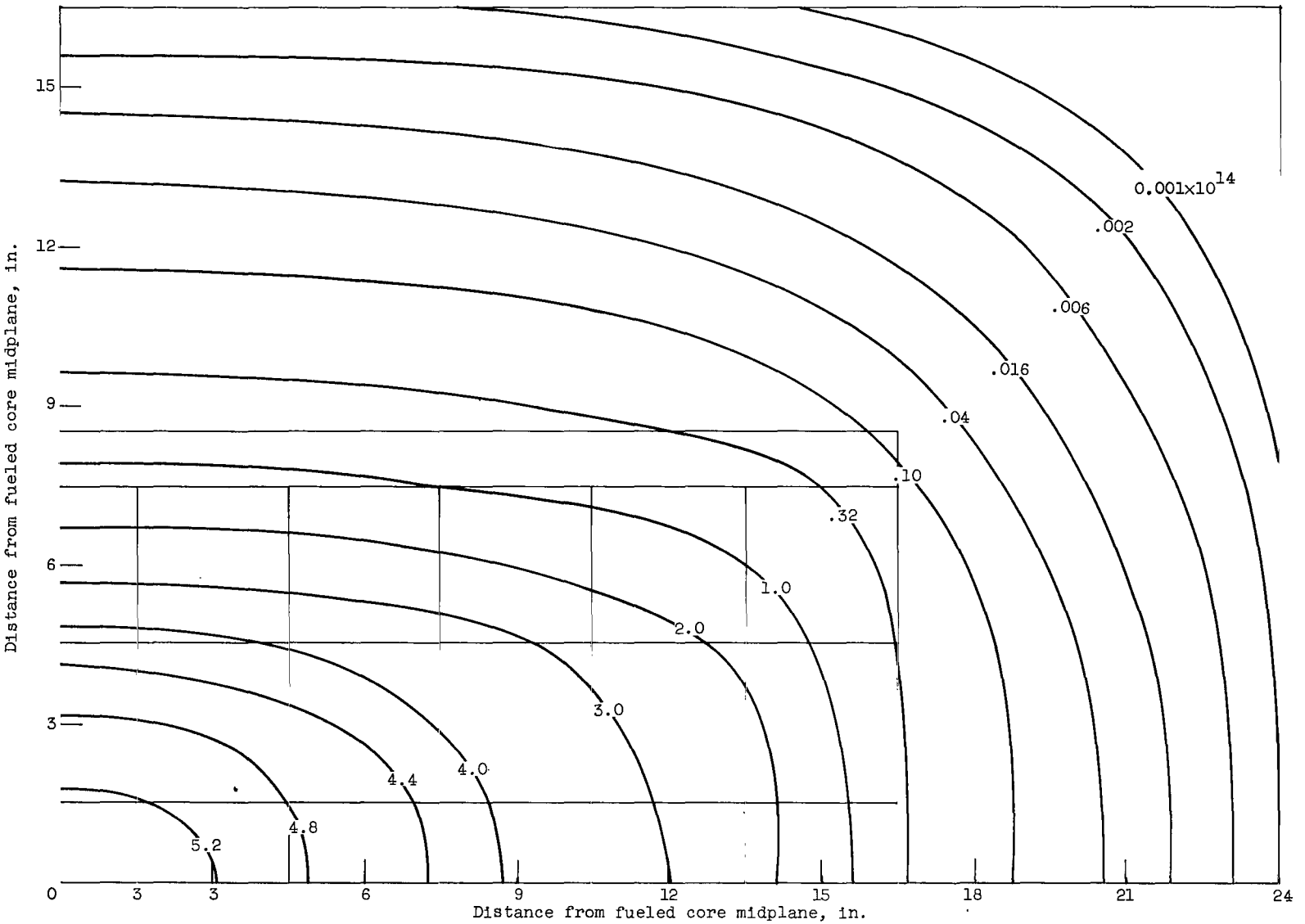

Figure 23. - Horizontal calculation of group 2 flux. Normalized to 60 megawatts of core power.

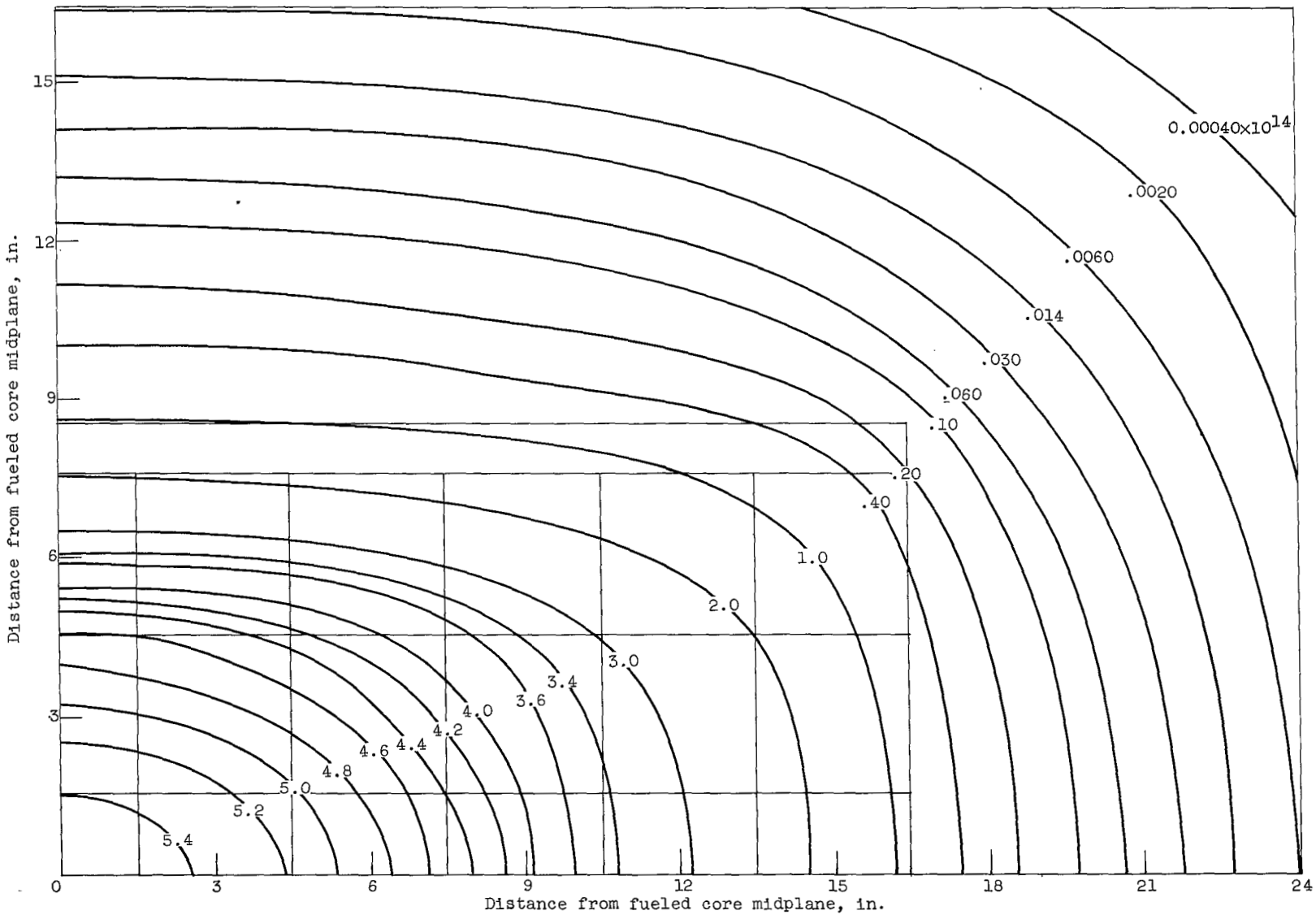

Figure 24. - Horizontal calculation of group 3 flux. Normalized to 60 megawatts of core power.

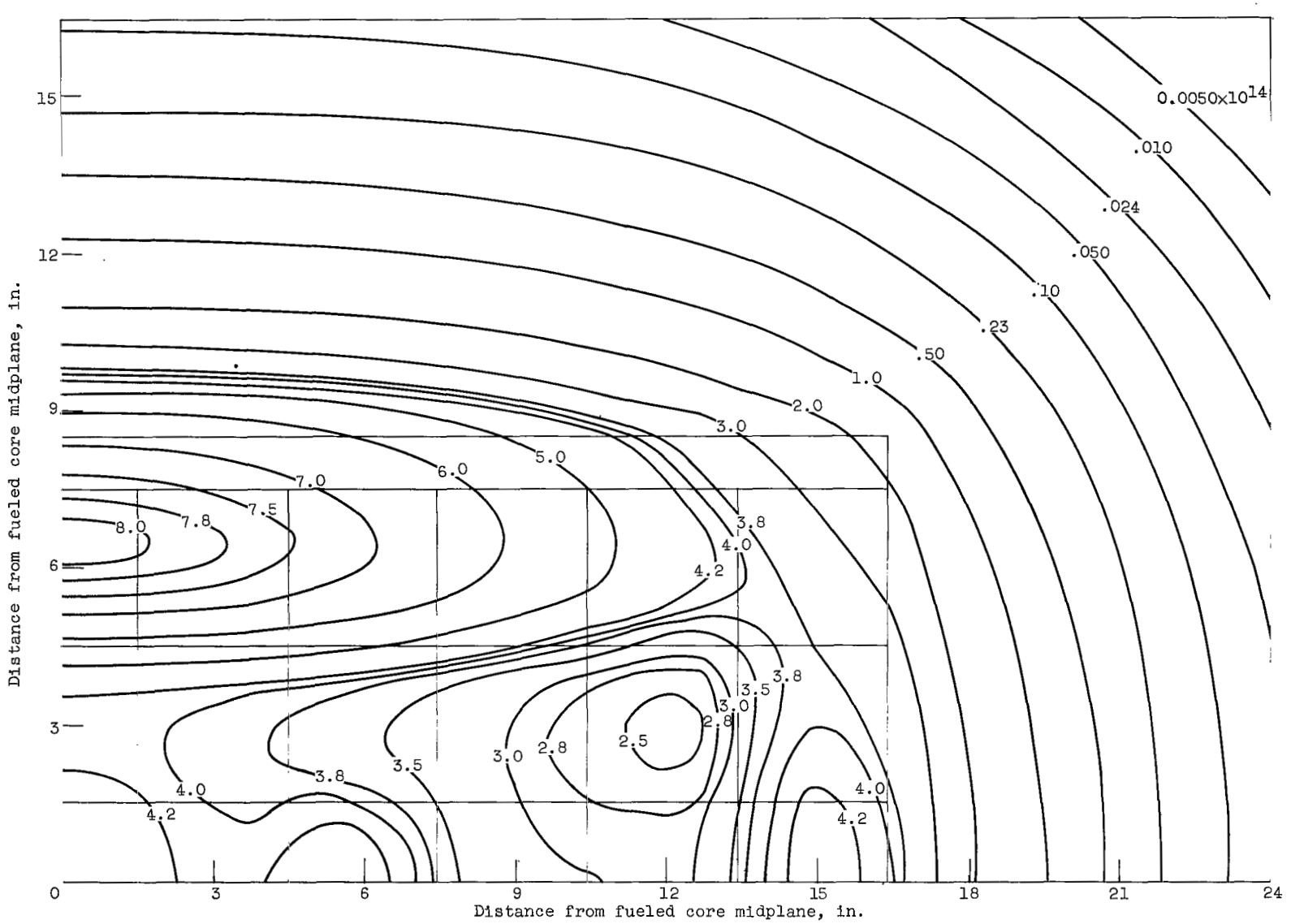

Figure 25. - Horizontal calculation of thermal flux. Normalized to 60 megawatts of core power.

"The aeronautical and space activities of the United States shall be conducted so as to contribute . . . to the expansion of human knowledge of phenomena in the atmosphere and space. The Administration shall provide for the widest practicable and appropriate dissemination of information concerning its activities and the results thereof."

—NATIONAL AERONAUTICS AND SPACE ACT OF 1958

NASA SCIENTIFIC AND TECHNICAL PUBLICATIONS

TECHNICAL REPORTS: Scientific and technical information considered important, complete, and a lasting contribution to existing knowledge.

TECHNICAL NOTES: Information less broad in scope but nevertheless of importance as a contribution to existing knowledge.

TECHNICAL MEMORANDUMS: Information receiving limited distribution because of preliminary data, security classification, or other reasons.

CONTRACTOR REPORTS: Technical information generated in connection with a NASA contract or grant and released under NASA auspices.

TECHNICAL TRANSLATIONS: Information published in a foreign language considered to merit NASA distribution in English.

TECHNICAL REPRINTS: Information derived from NASA activities and initially published in the form of journal articles.

SPECIAL PUBLICATIONS: Information derived from or of value to NASA activities but not necessarily reporting the results of individual NASA-programmed scientific efforts. Publications include conference proceedings, monographs, data compilations, handbooks, sourcebooks, and special bibliographies.

Details on the availability of these publications may be obtained from:

SCIENTIFIC AND TECHNICAL INFORMATION DIVISION

NATIONAL AERONAUTICS AND SPACE ADMINISTRATION

Washington, D.C. 20546